DEPARTMENT OF NATIONAL DEFENCE
CANADA

OPERATIONAL RESEARCH AND ANALYSIS

DIRECTORATE OF AIR OPERATIONAL RESEARCH

DAOR RESEARCH NOTE 94/5

FIRST-ORDER SIMULATION OF STREWN DEBRIS FIELDS ACCOMPANYING EXOATMOSPHERIC RE-ENTRY VEHICLE FRAGMENTATION BY HYPERVELOCITY IMPACT

by

Dr. Gregory W. Frank

SEPTEMBER 1994

OTTAWA, CANADA

National Defence   Défense nationale

Operational Research and Analysis

CATEGORIES OF PUBLICATION

<u>ORA Reports</u> are the most authoritative and most carefully considered publications issued. They normally embody the results of major research activities or are significant works of lasting value or provide a comprehensive view on major defence research initiatives. ORA Reports are approved by DGOR and are subject to peer review.

<u>ORA Project Reports</u> record the analysis and results of studies conducted for specific sponsors. This category is the main vehicle to report completed research to the sponsors and may also describe a significant milestone in ongoing work. They are approved by DGOR and are subject to peer review. They are released initially to sponsors and may, with sponsor approval, be released to other agencies having an interest in the material.

<u>Directorate Research Notes</u> are issued by directorates. They are intended to outline, develop or document proposals, ideas, analysis or models which do not warrant more formal publication. They may record development work done in support of sponsored projects which could be applied elsewhere in the future. As such they help serve as the corporate scientific memory of the directorate.

DEPARTMENT OF NATIONAL DEFENCE

CANADA

OPERATIONAL RESEARCH AND ANALYSIS

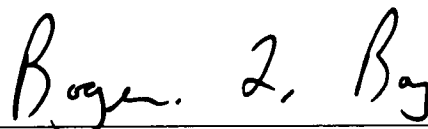DIRECTORATE OF AIR OPERATIONAL RESEARCH

DAOR RESEARCH NOTE 94/5

FIRST-ORDER SIMULATION OF STREWN DEBRIS FIELDS ACCOMPANYING EXOATMOSPHERIC RE-ENTRY VEHICLE FRAGMENTATION BY HYPERVELOCITY IMPACT

by

Dr. Gregory W. Frank

Recommended By: _____

Roger L. Roy, Director Air Operational Research

OTTAWA, CANADA   SEPTEMBER 1994

ABSTRACT

This report documents a computer-based model to simulate the strewn debris field resulting from exoatmospheric ballistic missile interception by a hypervelocity kinetic kill vehicle. The model supports a suite of simulations developed to augment policy or strategic studies by capturing the basic physics of missile defence. The model is intended to serve as a 'first order' approximation, describing physical processes at a level of detail sufficient to describe strewn field formation qualitatively. This report is a technical document of the physics underlying fragmentation and dispersion, and is intended for analysts working with or expanding the package. The fragmentation of ballistic missile re-entry vehicles is modelled using available information from satellite on-orbit and laboratory collisions. Atmospheric fragment re-entry is modelled using an exponentially dense ablative atmosphere model derived from meteor physics. Strewn field distributions are inferred through impact points across a range of fragment masses. Follow-on analysis packages compute and display mean and cumulative fragment densities accompanying multiple intercept scenarios. While this study does not address specific scenarios, several trends have emerged: interceptions may occur at altitudes of hundreds of kilometres, several hundred seconds before scheduled Re-Entry Vehicle impact. Such interceptions are often characterized by debris fields measuring several hundreds of kilometres across. It was found that, assuming uniform fragment distribution yields low mean fragment mass densities on the order of a few grams per square kilometre.

RÉSUMÉ

Ce rapport documente un modèle informatique qui simule l'étendue des débris résultant d'une interception exoatmosphérique d'un missile balistique par un véhicule cinétique hypersonique. Le modèle fait parti d'une classe de simulations qui capture la physique de la défense anti-missile et qui a été développé pour supporter les études stratégiques et politiques. Le processus physique de la formation de l'étendue des débris est décrit en assez de détails pour produire une approximation de premier niveau. Ce document technique de la physique de la fragmentation et de la dispersion des débris est pour l'usage des analystes travaillant avec le progiciel. La fragmentation du corps de rentrée d'un missile balistique est modélisé à l'aide d'information disponible sur les collisions de satellites et en laboratoire. La rentrée des fragments dans l'atmosphère est modélisé selon un modèle atmosphérique ablatif à densité exponentielle dérivé de la physique météorique. L'étendue des débris est déduite par les points d'impacts résultant de différentes masses de fragments. Les progiciels calculent et présentent les densités moyennes et cumulatives des fragments dans un scénario à interception multiple. Même si cette étude ne s'adresse pas à un scénario spécifique, certaines tendances en résulte: les interceptions peuvent se produire à des centaines de kilomètres d'altitude, plusieurs centaines de secondes avant l'impact du corps de rentrée. Ces interceptions se caractérisent par des étendues de débris mesurant des centaines de kilomètres. Si l'on suppose une distribution uniforme des fragments, on obtient une densité moyenne de la masse des fragment de l'ordre de quelque grammes par kilomètre carré.

EXECUTIVE SUMMARY

This Research Note documents work done in the Directorate of Air Operational Research, as part of an ongoing project to develop analytical tools to examine issues in Ballistic Missile Defence in support of potential policy studies. The tools are designed to assess the ability of a missile defence system to defend an extended area, and the consequences of that defence. This Note documents an analytical tool developed to assess some of the consequences of BMD by modelling the strewn debris field formed by re-entering missile fragments following interception by a very high speed Kinetic Kill Vehicle.

Current missile defence research is focusing on the use of direct-impact Kinetic Kill Vehicles for both Theatre and Intercontinental Ballistic Missile Defence. Advances in guidance, discrimination and sensor technologies have made possible missile defence through destructive interception, in which a small and fast Kinetic Kill Vehicle is used to physically collide with a ballistic missile or Re-entry Vehicle (RV). The kinetic energy accompanying a body-to-body impact at speeds of several kilometres per second is adequate to ensure RV destruction. Laboratory and range tests have indicated that an RV is likely to be fragmented into a very large number of small pieces, hurled away from the interception site at high speed by the energy of the collision. This raises questions in a policy or strategy venue: for example, given a successful interception, how many small or large fragments are likely to be produced, and where are they likely to land? What risk hazard is associated with falling debris? Can these hazards be managed by controlling the intercept location?

This report describes a computer-based package developed to address these questions by simulating the probable strewn debris pattern resulting from a hypervelocity missile/interceptor collision. The fundamental physical processes governing fragmentation, fragment re-entry and ground impact are modelled mathematically. The model is intended to serve as a 'first-order' assessment tool, modelling processes with sufficient detail to illustrate the central issues. It can either serve to augment policy or strategy studies, or it can be used as a precursor to more detailed engineering or systems-level simulations.

The text technically describes each fundamental process, its mathematical description and its incorporation into the simulation package. It is intended to be used by analysts working with or expanding the package. The remainder of the Executive Summary is a non-technical discussion of the model, its capabilities and first findings.

To illustrate the processes at work in forming a strewn field, consider a hypothetical intercept scenario: an Intercontinental Ballistic Missile (Re-entry Vehicle mass 1000 kg, speed at intercept 5 km/sec) is intercepted using a continental BMD system (Interceptor Vehicle mass 10 kg, speed 5 km/sec). We assume that Early Warning sensors have allowed the Interception Vehicle to be launched early enough to intercept

the Re-entry Vehicle at an altitude of several hundred kilometres, outside the Earth's atmosphere (exoatmospherically). Also assume for simplicity interception occurs head-on, with the interceptor striking the Re-entry Vehicle at a relative speed of 10 km/sec. The kinetic energy accompanying the collision is tremendous: the interceptor impacts with the energy equivalent of several fully-loaded C-130's travelling at takeoff speed. More than half of this energy goes into creating and dispersing fragments, ejected from the Re-entry Vehicle at speeds ranging from a few metres to several kilometres per second. The debris expands in a cloud around the RV trajectory, spreading out uniformly about the original trajectory until it reaches the Earth's atmosphere at an altitude of about 100 km. The atmosphere at this altitude is sufficiently dense to begin decelerating lighter fragments; heavier fragments are decelerated later in the denser atmosphere encountered at lower altitudes. As fragments are decelerated, any lateral velocity they may have with respect to the Earth's surface is reduced. Lighter fragments are decelerated most quickly, striking the Earth further uprange of heavier fragments. The debris field thus produced has a complicated structure, with fragments of different masses distributed across it in a complex manner dependent upon the missile's position and velocity at intercept.

This process is modelled here in three distinct modules: *fragmentation, re-entry* and *field formation*. The fragmentation module simulates the probable fragment mass and ejection velocity spectrum accompanying interception. These are derived from the available literature on satellite laboratory tests and on-orbit collisions. Much of this work is necessarily speculative: the dynamics of hypervelocity collisions and material behaviour under extreme stresses and loading are not well understood. However, an adequate collision database has been built up to allow dominant trends and effects to be modelled.

Collision results in the creation of a large number of fragments. Laboratory and range evidence both suggest that a large fraction of the RV/IV mass is converted into small fragments (on the order of a few grams or less) and ejected at speeds of several kilometres per second relative to the original RV trajectory. Larger fragments which survive the impact are ejected at speeds of a few metres per second. This forms a debris cloud travelling along the original RV trajectory and expanding outwards at several kilometres per second. For the case described above, interception may occur a few hundred seconds before the scheduled RV impact; thus the debris cloud may measure from several hundred to a thousand kilometres across by the time it encounters the upper atmosphere. Fragment behaviour during re-entry is modelled using the same equations of motion governing missile re-entry. Motion is determined by considering the forces due to gravity and the atmosphere acting on each fragment at each step of its trajectory. The atmosphere model describes the exponential density variation of the atmosphere with altitude. The possibility of fragment mass ablation due to atmospheric friction is considered by incorporating a mass loss model from meteor re-entry physics.

Several fragments with a range of masses are simulated, their re-entry trajectories calculated and their impact points stored. These are used to estimate the probable extent of the strewn debris field resulting from either single or multiple intercepts. Graphics packages have also been developed to display fields.

Although this study does not address specific intercept scenarios, several trends have emerged which deserve comment. The intuitive description of fragmentation and cloud size are borne out in simulation: intercepts occurring hundreds of seconds before the scheduled RV impact are usually characterized by large debris fields. These fields can be several hundred to a thousand kilometres across. Assuming a constant fragment distribution gives fragment densities on the order of a few grams per square kilometre. While the exact size and shape of the fragment field is sensitively dependent upon the intercept conditions, such low densities are usually typical of long-range intercepts.

In summary, this model serves as a basic assessment tool, providing estimates of strewn debris fields resulting from ballistic missile intercepts. The constituent processes are modelled at a level of detail sufficient to augment strategy or policy studies, or to serve as a precursor to more detailed systems or engineering-level investigations.

TABLE OF CONTENTS

LIST OF ILLUSTRATIONS

LIST OF ABBREVIATIONS

BMD	Ballistic Missile Defence
CN	Cumulative Number
DAOR	Directorate of Air Operational Research
DGOR	Director General Operational Research
DREV	Defence Research Establishment Valcartier
E^2I	Exoatmospheric/Endoatmospheric Interceptor
ERIS	Exoatmospheric Re-entry vehicle Interceptor System
g	Sea-level acceleration due to gravity
gm	Gram
GBI	Ground-Based Interceptor
GPS	Global Positioning System
HEDI	High Endoatmospheric Defence Interceptor
IC	Initial Conditions
ICBM	Inter-Continental Ballistic Missile
IR	Infrared
IV	Interception Vehicle
kg	Kilogram
KITE	Kinetic energy kill vehicle Integrated Technology Experiment
KKV	Kinetic Kill Vehicle
km	Kilometre
LEAP	Lightweight Exoatmospheric Projectile
m	Metre
NMD	National ballistic Missile Defence
RV	Re-entry Vehicle
TBM	Theatre (Tactical) Ballistic Missile
THAAD	Theatre High Altitude Area Defence
TMD	Theatre ballistic Missile Defence

FIRST-ORDER SIMULATION OF STREWN DEBRIS FIELDS ACCOMPANYING EXOATMOSPHERIC RE-ENTRY VEHICLE FRAGMENTATION BY HYPERVELOCITY IMPACT

I. INTRODUCTION

BACKGROUND

PROJECT BACKGROUND

1.   This Research Note documents work done in the Directorate of Air Operational Research (DAOR) as part of DGOR Activity 23213 (Analysis of Space-Related and Space-Systems). A series of projects under this Activity has developed a set of computer-based simulations on the physics of space-based and space-related defence systems, including:

       a.   Theatre and Intercontinental Ballistic Missile (TBM and ICBM respectively) trajectory simulations (Reference 1);
       b.   ballistic missile interception models (Reference 2);
       c.   Ballistic Missile Defence (BMD) simulations (Reference 3); and
       d.   post-intercept strewn debris field simulation following Re-Entry Vehicle/ Interceptor Vehicle (RV/IV) interception.

The goal of this suite is twofold: to examine the ability of a BMD system to defend an extended area, and to determine the consequences of that defence. The suite is intended to augment policy or strategic studies by capturing the basic physics of missile defence.

2.   This Note documents the final item listed above: the simulation of the fragmentation and eventual strewn debris field resulting from the kinetic kill of a long-range ballistic missile by hypervelocity impact with a small interceptor mass. The strewn field simulator supports the analysis of the consequences of BMD.

PROJECT OUTLINE

3.   It was decided to construct a computer-based package to simulate the probable fragmentation and strewn debris pattern resulting from a hypervelocity missile/interceptor collision. The physics of hypervelocity collision and fragmentation, atmospheric fragment re-entry and strewn field formation are modelled mathematically. The model is intended to serve as a 'first order' approximation, describing basic physics at a level of detail sufficient to describe the principal processes at work. As such it can serve to augment policy and strategy studies, or it can be used as a precursor to a more detailed engineering or systems simulation.

AIM

4.   This Research Note documents the simulation package and paradigms used to model the fragmentation and strewn debris field. It is intended primarily to aid analysts in understanding, using and modifying the package.

BALLISTIC MISSILE INTERCEPT TECHNOLOGIES

5.   Current United States Ballistic Missile Defence (BMD) plans call for Kinetic Kill Vehicles (KKVs) for both Theatre and National Missile Defence (TMD, NMD respectively) (References 4,5,6), with much current activity directed towards near-term development of usable systems (References 7,8,9). KKVs will consist of lightweight intercept vehicles launched atop multi-stage solid-propellant anti-ballistic missiles. Dependent upon the BMD system configuration and ballistic missile profile, TMD and

NMD intercepts will occur during missile midcourse or re-entry at altitudes of tens to several hundreds of kilometres, respectively. The KKV proper will consist of sensors, guidance and navigation modules combined into a 10-20 kg package (Reference 10). The following anti-ballistic missile programmes demonstrate present and near-term KKV interceptor capabilities:

    a.   Ground-Based Interceptor (GBI);
    b.   Endo-Exoatmospheric Interceptor (E^2I); and
    c.   Theatre High Altitude Air Defence (THAAD).

GROUND-BASED INTERCEPTOR (GBI)

6.   The Ground-Based Interceptor is a long-range two-stage solid propellant anti-ballistic missile.[1] The GBI will intercept RVs during missile midcourse at altitudes greater than 200 km and ranges from 200 km to 2000 km, with a launch velocity of about 4 km/sec. With a range of several thousand km a GBI would be capable of acting within a continental defence system. The programme builds on the Exoatmospheric Re-entry vehicle Interceptor System (ERIS) programme, started in 1986.

7.   The GBI KKV mass is to be between 10 kg and 20 kg. Target discrimination will be distributed between ground processors and onboard sensors, with terminal maneouvers performed by liquid-fuel thrust and divert engines. An inflatable plastic/mesh kill enhancement device may be used to enlarge the KKV cross section. It is possible that the KKV could be based on the existing Lightweight ExoAtmospheric Projectile (LEAP) technology programme (Reference 11). The KKV would be carried in a two-stage boost vehicle about 5m long with 800 kg launch weight. Midcourse guidance and supplemental discrimination could be through inertial, Global Positioning System (GPS), star tracking and command updates.

---

[1]   GBI information is summarized from Reference 10.

ENDO-EXOATMOSPHERIC INTERCEPTOR (E^2I)

8.   The E^2I programme is parallel to the GBI.[2] E^2I is derived from the High Endoatmospheric Defence Interceptor Kinetic energy kill vehicle Integrated Technology Experiment (HEDI/KITE), begun in 1986. E^2I aims at developing a ground-based interceptor with 6.5 km/sec launch velocity and range out to 5000 km. The interceptor would be capable of performing interceptions in space (exoatmospheric) and at altitudes as low as 15 km (endoatmospheric). High speed atmospheric operation is permitted by advanced thermal shielding and IR sensor cooling systems. The E^2I interceptor is similar to the GBI interceptor, with a mass of 10-20 kg and multi-colour cooled IR sensor. It will be carried by a 6.5 m, 1200 kg two-stage solid propellant missile.

THEATRE HIGH ALTITUDE AREA DEFENCE (THAAD)

9.   THAAD is a medium-range ground and ship-based theatre defence missile.[3] THAAD is intended to provide first line defence as an upper layer above Patriot, Hawk or Standard systems. THAAD will use a KKV atop a 5m long 1000 kg two-stage solid propellant missile. It is expected to have an intercept range of about 150 km and mesoatmospheric intercept altitude range of 15 to 100 km. The THAAD KKV is expected to weigh from 10 to 15 kg and will be derived from current or near-term LEAP technology, funded to support the E^2I programme. KKV guidance would be through inertial, GPS and command updates. Terminal guidance is likely to be dual mode, using both active radar and multispectral IR seekers.

---

[2] E^2I information is summarized from Reference 10.

[3]   THAAD information is summarized from Reference 10.

KKV PHYSICS SIMULATION

10.   This section summarizes the physics encapsulated by the hypervelocity intercept simulation. Little is known about materials properties under the extreme stresses and loading conditions experienced during collisions at relative speeds on the order of 10 km/sec. Necessarily much contained here is speculative and subject to debate; however the current understanding of hypervelocity impacts is sufficiently well established to support the simulation's goal of providing a 'first order' debris distribution model.

11.   The debris simulation package is built around three principal modules (Figure 1), each simulating a distinct phase of the dispersal process:

a.   *Fragmentation:* fragmentation following the RV/IV collision is modelled using ejecta mass and velocity distributions derived from the available information on on-orbit and test range collisions.

b.   *Fragment re-entry:* post-intercept fragments fall under gravity through an increasingly dense model atmosphere until ground impact.

c.   *Strewn debris field formation:* the size, shape and orientation of the IV/RV strewn debris field is inferred through the ground distribution of test fragments. Post-processing is performed to determine the geographic mean fragment mass density distribution accompanying specific missile launch/defence system pairs.

The following section discusses the main physical and mathematical components of each of the three phases. They are intended to acquaint the model user with the processes at work, prior to discussing their simulation.

Fragmentation

- RV/IV Initial Conditions
- Fragmentation Database
- Fragment production
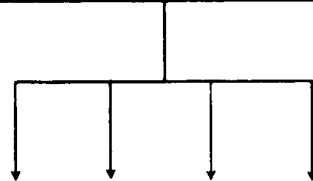
Fragment Re-Entry

- Fragment Initial Conditions
- Atmospheric Re-Entry
  (Deceleration, Ablation)
- Ground Impact

Strewn Field Formation

- Fragment Ground Location
- Strewn Field Size, Shape, Density.

Figure 1: Strewn Debris Field -
Principal Modules

II. METHOD

12.   Strewn debris field formation is modelled as three distinct processes: impact fragmentation, atmospheric fragment re-entry, and strewn field formation and analysis. This section describes each module, and introduces the relevant physical and mathematical background. It concludes with a description of the modules' inclusion in the simulation package.
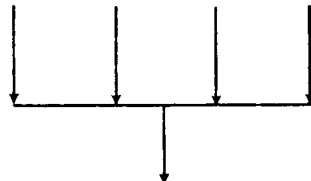
FRAGMENTATION MODULE

INTRODUCTION

13.   The dynamics of very high speed collisions are not well understood. Supersonic impact speeds can result in the creation of discontinuous shock and pressure fronts; as impact shocks propagate through a medium at the speed of sound in that medium, these may be accompanied by novel mechanical, elastic and thermal effects. Ballistic missile intercepts will occur at speeds on the order of ten times that of shock propagation, speeds which cannot be easily duplicated under laboratory conditions.

14.   The fragmentation module is intended to simulate the mass and speed distribution of the post-intercept ejecta, at a level of detail sufficient to indicate the likely extent of the strewn debris field. The module is designed to provide a first approximation to field shape and extent, using simple models and assumptions. A detailed description of the intercept would require extensive modelling of both the ballistic missile and the interceptor's materials and construction, coupled with a simulation of materials behaviour under extreme stresses and loading conditions. The fragmentation model used here computes ejection speeds using a simplified model based on available data derived from satellite orbital collisions and existing laboratory and range tests. The model does not include details on RV or IV construction beyond their impact mass and mean density: this results in a probabilistic description of the debris cloud and strewn debris field.

15. A recent survey article (Reference 12) reviews several studies which attempt to characterize the particulate distributions of debris resulting from hypervelocity impact. The debris cloud thus produced defines the initial conditions for debris hazard assessment. The key parameters of the collisional initial conditions are:

a. the *velocity distribution*, determining the subsequent spatial and temporal evolution of the debris cloud;

b. the *mass distribution*, determining the lethality of subsequent impacts; and

c. the *ballistic coefficient distribution* and its secondary effects upon the velocity and mass distributions through atmospheric drag.

16. Fragmentation occurs through kinetic energy deposition. In the RV rest frame, the kinetic energy of the interceptor is

$$T = \frac{1}{2}mv^2 , \tag{1}$$

where (m,v) are the interceptor mass and speed, respectively. The kinetic energy accompanying hypervelocity impact goes into heat, light, deformation, fragmentation and debris spread. Empirical evidence suggests that if two colliding objects are of comparable mass, the energy available for debris spread is about half the available energy. If the projectile mass is small in comparison with the target, then almost all of the energy goes into the spread of debris (References 12,13).

17. The current understanding of debris distribution is described below. Some care must be taken in implementation, however, as there is much uncertainty in the mass and velocity distribution models. Care must be taken when extrapolating these results to higher speeds and energies, and much analytical work remains to be done to determine which parameters may be accurately scaled. These caveats should be recalled throughout this section.

VELOCITY DISTRIBUTION

18.   The particulate velocity distribution is based largely on empirical data derived from test ranges and on-orbit collisions. Empirical evidence shows that large fragments are ejected from a hypervelocity collision at about 10 m/sec, while smaller fragments are ejected at much faster speeds on the order of 4-11 km/sec. The maximum observed ejecta velocity for smaller particles is normally about 1.3 times the relative projectile velocity.

19.   The available empirical data is well modelled by the velocity distribution

$$\log(\frac{V}{V_p}) = \begin{cases} A - B(\log\frac{d}{d_m})^2, & d > d_m, \\ A & , d < d_m. \end{cases} \tag{2}$$

with:

V   the fragment ejection velocity (m/sec);
V_p the relative intercept velocity (m/sec);
d   the fragment diameter (m);
d_m $= E_p^{1/2}/6.194 \times 10^7$ m an empirical scaling constant;
E_p the projectile energy (J).

Values of A are in the range of 0.1-0.25, with nominal mean value <A> = 0.225. Values of B on the order of 0.10 are generally accepted. Data from a variety of observed on-orbit breakups shows good correlation with this model (References 12,13).

20.   Figure 2 shows families of fragment ejecta mass/ejection speed distribution curves accompanying variations in model parameters. The default parameter set is:

Target mass: 1000 kg;
Impactor mass: 10 kg;
Impactor speed: 10 km/sec with respect to target rest frame;
A = 0.225;
B = 0.10.
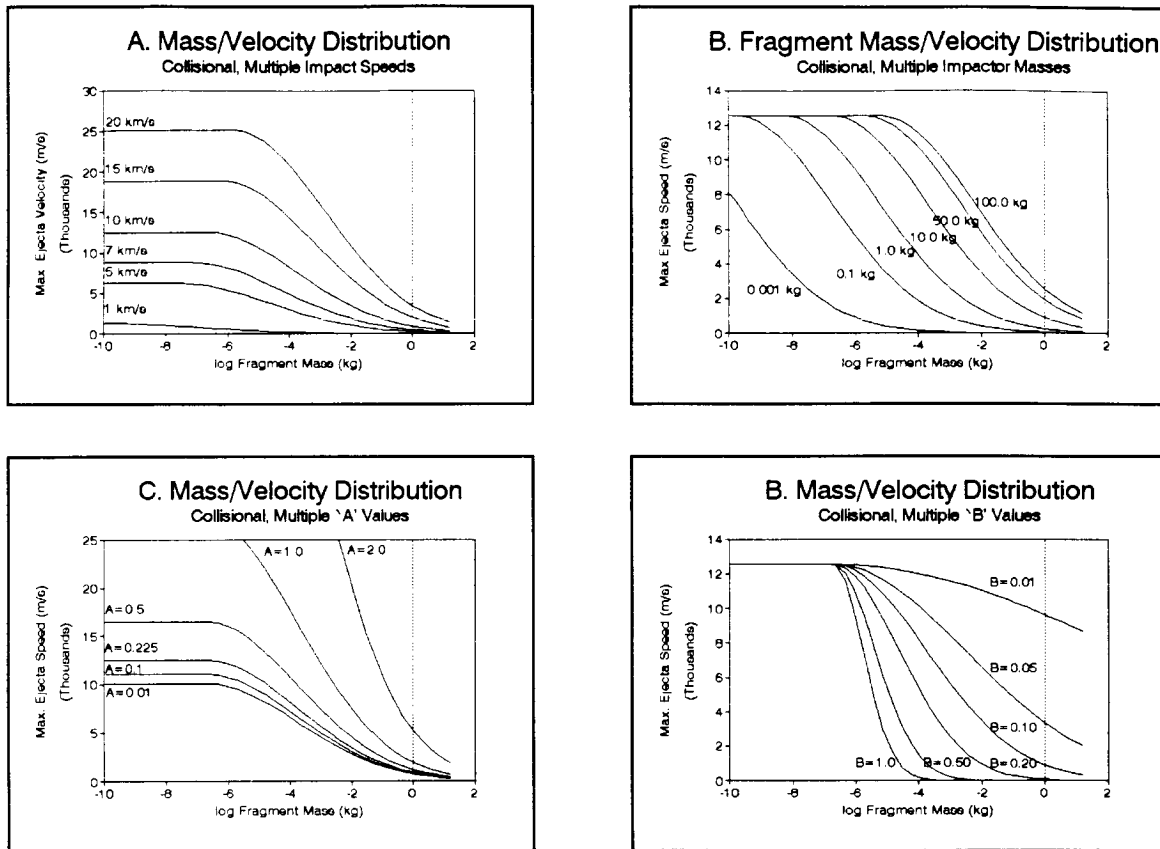
Figure 2: Collisional Fragmentation Mass/Velocity Distribution

21.   Figure 2A shows the family of curves resulting from impact speeds from 1 km/sec through 20 km/sec. The decimal logarithm of ejected fragment mass is plotted against the greatest expected ejecta velocity using Equation (2). Typical velocity values accompanying ballistic missile intercept range from 4 km/sec (TBM interception) through 12 km/sec (ICBM interception). Curves are displaced upwards with increasing impact speed, as increased kinetic energy deposition provides more energy for faster fragment ejection. Figure 2B indicates response across a range of impactor masses. Curves are displaced horizontally to the right with increasing impactor mass, as ejection energy available for a constant fragment mass increases with impactor mass. Figures 2A,2B demonstrate the heuristic accompanying Equation (2): the greatest expected fragment ejection velocity is dependent only upon impactor speed.

22.   The lower figures indicate distribution response with respect to variation of the empirically derived parameters {A,B}. The lower left figure shows distribution curves accompanying variation in A over a range (0.01-2.0). Increasing A increases the ejection velocity for a given fragment mass, and thus controls the distribution amplitude. The nominal value of A=0.225 is shown. The lower right figure shows curves accompanying variation in B over a range (0.01-1.0). Increasing B decreases the ejection velocity for a given fragment mass, below maximum ejection velocity, and thus controls the fragment velocity dispersion. The nominal value of B=0.10 is shown.

23.   Figure 3 shows the conceptual information flow for the fragmentation module. RV and IV initial conditions and mass are used to generate a set of initial conditions for fragments across a range of masses. Sets of constant-mass fragments are assigned spherically symmetric ejection velocities with respect to the RV/IV Centre of Mass (CM).
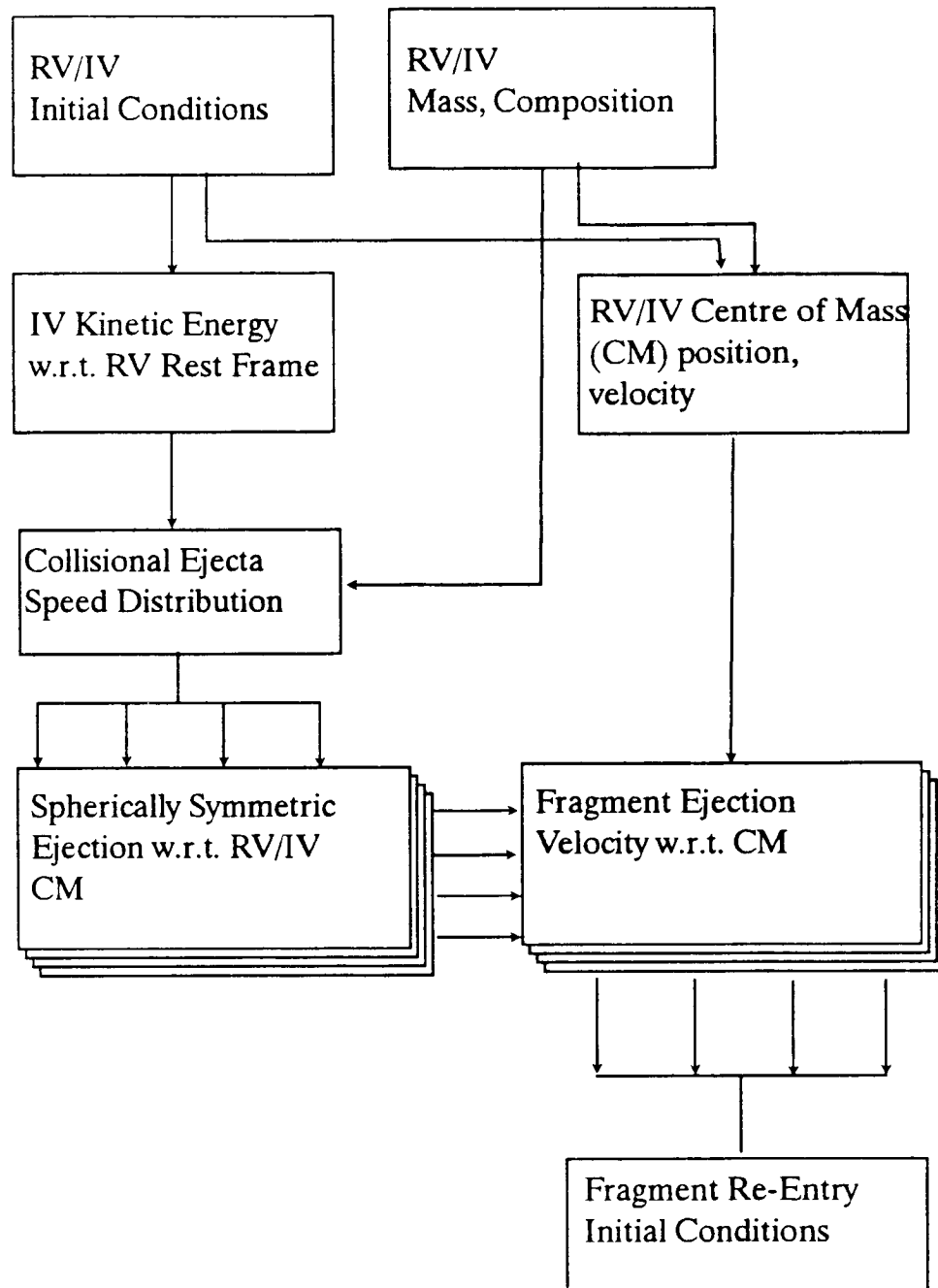
Figure 3: <u>Fragmentation Module - Conceptual Flow</u>

OTHER COLLISIONAL DISTRIBUTIONS

Mass Distribution

24.   Empirical studies have provided a useful heuristic concerning the ejecta mass distribution: the total ejecta mass for an on-orbit collision between a small fragment and a satellite at a relative speed of 10 km/sec is about 115 times the impactor's mass. Early studies of hypervelocity impacts with a spacecraft wall established a power law mass distribution:

$$CN = aM_f^{-b}, \qquad (3)$$

where CN is the cumulative number of fragments with mass greater than M_f, and (a,b) are constants of order 10 and 1 respectively. Further research has indicated a variety of alterative functional forms, including

$$CN_2 = a\left(\frac{M_f}{M_e}\right)^{-b},$$

$$CN_3 = \exp\left(c - d(\log(\frac{M_f}{M_e}) + e)^2\right), \qquad (4)$$

$$M_e = kV^2,$$

for various values of (a,b,c,d,e,k), as well as parabolic, hyperbolic and hypertrigonometric distributions. McKnight (References 12,13) notes that parameter values are very sensitive to the error estimation method used, with estimates varying by over 50% when slightly different tolerances are imposed.

25.   Explosive fragmentation is modelled much as collisional fragmentation: it is based on the assumption that if the projectile energy is large enough to cause complete target fragmentation, the ejecta mass follows a power law and the remainder breaks up in an explosion. The explosive mass distribution is usually taken as exponential, based on fragmentation tests during the 1960's with an Atlas booster:

$$CN_{Exp} = A'M_b e^{-B'\sqrt{M_f}},\qquad(5)$$

M_b the mass available for breakup, and (A',B') having values on the order of (0.005, 0.03). This functional form was supported in a series of experiments conducted at Defence Research Establishment Valcartier (DREV) (Reference 14), and by analyses performed by TRW to simulate the fragmentation of a launch vehicle from a purely analytic code (related in Reference 12).

26.   Related to the mass distribution is the number distribution: the number of large mass fragments produced by a hypervelocity impact event is found to scale as

$$N > 1.0^{-3}M_t = 5\sqrt{\frac{E_p}{M_t}}.\qquad(6)$$

Ballistic Coefficient Distribution

27.   The ballistic coefficient is defined as

$$BC = C_d X/M,\qquad(7)$$

where C_d is the drag coefficient, X the mean cross-sectional area and M the fragment mass. The ballistic coefficient determines the fragment's response to atmospheric drag. Ballistic coefficients of observed orbital fragments are inferred through their radar cross section. Assuming a circular cross section, the ballistic coefficient as a function of fragment diameter d is

$$BC = (1728/f)d^{2-g},\qquad(8)$$

where f= 10,000-60,000 and g = 2.25-2.5. This equation has not been validated and must be used carefully.

BALLISTIC FRAGMENT RE-ENTRY MODULE

INTRODUCTION

28.   Following fragmentation by hypervelocity collision, ejected fragments follow ballistic trajectories perturbed by the ejection velocity about the original RV trajectory. As fragments enter the increasingly dense atmosphere, the local air density becomes sufficiently high to perturb and decelerate re-entering fragments further. The extent of the atmospheric deceleration and trajectory perturbation is a function of fragment size, shape, composition, re-entry path and speed. The trajectory simulation module models fragment re-entry using equations of motion derived from meteoric and ballistic missile re-entry.

29.   This analysis builds upon an early treatment of the general ballistic missile re-entry problem (Reference 15). In that work, Allen and Eggers performed a simplified analysis of the velocity and deceleration profiles of re-entering ballistic missiles. It was found that, for high supersonic speeds and missile mass, the gravity force is negligible in comparison to the aerodynamic drag. The maximum height of missile deceleration is dependent only on fragment mass, re-entry speed and flight-path angle.

Equations of Motion

30.   Let {xyz} denote a topocentric-horizon coordinate system with origin **O** attached to an observer stationary on the surface of the Earth, with axes along the South, East and geocentric Up directions (Reference 16). Consider a body of mass m entering the atmosphere from some initial height z_0 and velocity $\mathbf{v}_0$. Let the velocity at altitude z be $\mathbf{v}$, and the angle of approach to the horizontal be θ. For simplicity let $\mathbf{v}$ be confined initially to the SZ-plane. Then the re-entry equations of motion can be written

$$\frac{d^2z}{dt^2} = -g + \frac{C_D \rho v^2 A}{2m} \sin\theta ,$$

$$\frac{d^2x}{dt^2} = \frac{C_D \rho v^2 A}{2m} \cos\theta , \qquad\qquad (9)$$

where

C_D is the body's drag coefficient (dimensionless);

v the body's speed (m/sec);

A the reference area for drag evaluation (m^2);

m the mass of the body (kg);

ρ the mass density of the air (kg/m^3);

g the acceleration due to gravity (m/sec^2);

x,z the horizontal and vertical distance from the point of impact with the Earth (m); and

θ the angle between the flight path and the local horizon (radians).

31.   Equations (9) describe fragment ballistic re-entry into the atmosphere. A further equation governs fragment mass ablation due to atmospheric friction (Reference {R.11}):

$$\frac{dm}{dt} = \begin{cases} -\dfrac{C_H \rho A}{2\zeta}\left(v^2 - v_{CR}^2\right), & v > v_{CR}, \\[2mm] 0, & v < v_{CR} \end{cases}$$

$$= -\frac{C_H \rho A}{2\zeta}\left(v^2 - v_{CR}^2\right) H(v - v_{CR}), \qquad\qquad (10)$$

where

C_H is the heat transfer coefficient; a function of speed, altitude and body size, on the order of 0.01-0.6;

ζ heat of ablation; a combination of heat of fusion and heat of vaporization, typically on the order of 5×10^6 J/kg; and

v_{CR} critical velocity below which no ablation occurs (experimentally estimated near 3 km/s for steel pellets),

and H(z) is the Heaviside step function.

32.   For simplicity, assume the drag coefficient and the acceleration of gravity to be constant over altitudes of interest. In actuality, the drag coefficient is a function of Mach and Reynolds number; assuming constant drag is generally valid at high Mach numbers so long as pressure drag dominates. Assuming constant gravitation acceleration introduces a small error, the variation of gravitational acceleration over the 100 km above the Earth's surface is

$$\delta g = \delta \left(\frac{GM}{r^2} \right)_{r=R_E} = -2 \frac{GM}{R_E^3} \delta r$$

$$= -2g \frac{\delta r}{R_E} \approx -0.03g \, , \tag{11}$$

where

R_E $= 6.378137 \times 10^6$ m, the mean Earth radius (WGS84, Reference 17); and
GM $= 3.986012 \times 10^{14}$ m³/sec² the equivalent Earth gravitational mass (Reference 16).

33.   The exact solution of Equations (9) is formidable. Consider first the simplified case in which the body descends vertically through an exponentially dense atmosphere:

$$\rho = \rho_o e^{-\beta z}, \tag{12}$$

where ρ_o and β are constants, on the order of 1 kg m⁻³ and 10^{-4} m⁻¹, respectively (more precise values will be presented below).

34.   Equations (9) then reduce to the single equation

$$\frac{d^2z}{dt^2} = \frac{dv}{dt}$$

$$= -g + \frac{C_D \rho_o A}{2m} e^{-\beta z} v^2. \tag{13}$$

Defining

$$\xi = v^2,$$
$$\frac{dv}{dt} = \frac{dv}{dz}\frac{dz}{dt} = v\frac{dv}{dz} \tag{14}$$
$$= \frac{1}{2}\frac{d\xi}{dz},$$

gives the linear first-order differential equation

$$\frac{d\xi}{dz} - \frac{C_D\rho_\sigma A}{m}e^{-\beta z}\xi + 2g = 0, \tag{15}$$
$$\xi(h) = v_o^2.$$

where the body has initial velocity v_0 at altitude h. The solution of this equation follows multiplication by the integrating factor

$$I(z) = \int_z \exp-\frac{C_D\rho_\sigma A}{m}e^{-\beta z_o}\,dz_o, \tag{16}$$

to form

$$\frac{d}{dz}\{I(z)\xi(z)\} = -2g\,I(z), \tag{17}$$
$$\xi(h) = v_o^2.$$

35.   The general solution of this is (Reference 18)

$$\xi(z) = \frac{-2g}{I(z)}\left(\int_z I(z_0)\,dz_0 + C\right), \tag{18}$$

where C is a constant of integration determined by the initial conditions. Integration is accomplished by expanding the inner exponential in a Taylor series to produce the series solution

$$\xi(z) = v^2(z)$$

$$= \exp\frac{\alpha}{\beta}(e^{-\beta h} - e^{-\beta z})v_o^2$$

$$- 2g\exp(-\frac{\alpha}{\beta}e^{-\beta z})$$

$$\cdot\left\{(z-h) + \sum_{n=1}^{\infty}\frac{\alpha^n}{n\beta^{n+1}}\frac{1}{n!}(e^{-n\beta h} - e^{-n\beta z})\right\},$$

$$\alpha = \frac{C_D\rho_0 A}{m}.$$

(19)

The deceleration experienced by the vertically descending body follows as

$$\frac{d^2z}{dt^2} = \frac{dv}{dt}$$

$$= \frac{1}{2\sqrt{\xi}}\frac{d\xi}{dt}$$

$$= -g + C_D\rho_o\frac{A}{2m}e^{-\beta z}\xi.$$

(20)

36. For a vertically descending 1 kg body with reference area 0.01 m² and $C_D = 1$, atmospheric deceleration at 5β altitude at 4 km/sec is on the order of 500 m/sec² ~ 50g. Hence gravitational acceleration may be negligible in a first approximation of high speed re-entry. For the nominal ablation values following Equation (10) the mass ablation at this speed and altitude is on the order of 10^{-2} kg/sec.

Atmospheric Model

37. This study assumes the following in modelling the Earth's atmosphere:

    a.   Nonrotating atmosphere;
    b.   Exponential density atmosphere.

Hypervelocity re-entry analysis usually assumes the Earth's atmosphere to be nonrotating, simplifying the dynamics of spacecraft-atmosphere interaction during launch and re-entry phases. Assuming a nonrotating atmosphere introduces only a small error; the maximum atmospheric rotational speed on the Earth's equator,

$$v_{Equator} = R_{Earth} \omega_{Rot},$$
$$= 465.02 \, m sec^{-1},$$
(21)

is about 5% of the low-altitude orbital speed[4]

$$v_{CS} = \sqrt{\frac{\mu}{R_E}}$$
$$= 7.905 x 10^3 \, m \, sec^{-1},$$
(22)

with $\omega = 7.292115 x 10^{-5}$ rad/sec the mean Earth angular velocity. Assuming a drag force quadratic in velocity gives a maximum 10% correction to the total aerodynamic forces from atmospheric rotation (Reference 19).

38.   Atmospheric density is assumed to decrease exponentially with altitude. This frequent assumption greatly simplifies analytical and computational analysis (References 19,20,21,22). At height z, atmospheric density ρ has the form of Equation (11), with sea level atmospheric mass density and scale height determined experimentally.

39.   Vinh *et al* (Reference 19) discuss the nuances of this assumption, which is based on the ideal gas law and the pressure equation of state for a static atmosphere. The exponential distribution follows by assuming an isothermal atmosphere (dT/dr = 0) in a uniform gravitational field. Refinements to this approximation include locally exponential models in which the atmosphere is partitioned into concentric shells with piecewise continuous exponential densities. These refinements must be weighed against the added complexity and minimal additional insight. Seasonal and geographic temperature

---

[4]   Derivation: Bate, Mueller and White 16, pp. 33-34.

variations are on the order of 15% of the mean atmospheric temperature (240 degrees Kelvin), inducing scale height variations on the order of 5% (Reference 19). This variation is not considered large enough to warrant the increase in model complexity.

40. Values for sea level atmospheric density and scale height may be found in standard references or computed from standard sources. A least squares fit to density data from Reference 20 gives

$$\rho_0 = 1.225 \pm 0.05 \; kg \; m^{-3}, \tag{23}$$
$$H = 7.2 \pm 0.1 \; km,$$

These values are consistent with those of the literature (References 19-22).

Atmospheric Deceleration Profile

41. The argument above shows that decelerations accompanying high entrance speeds may reach large values compared with the acceleration due to gravity. This suggests that the gravity term may be neglected without seriously affecting the results. In this case the flight path is essentially a straight line. The altitude at which the greatest deceleration occurs follows from this as

$$h = \frac{1}{\beta} \ln \frac{C_D \rho_o A}{\beta m \sin\theta_E}, \tag{24}$$

which depends only on the size and mass of the re-entry body, but not its initial velocity. For the 1 kg test body in the example above, maximum deceleration occurs at 40-50 km altitude.

NUMERICAL INTEGRATION

42. The ballistic re-entry Equations of motion (9,10) are a set of first and second-order nonlinear ordinary differential equations (ODE). Their numerical solution is facilitated by rewriting as a set of coupled first order ODEs:

$$\frac{dx}{dt} = v_x,$$

$$\frac{dz}{dt} = v_z,$$

$$\frac{dv_x}{dt} = \frac{C_D \rho A}{2m} \left(v_x^2 + v_z^2 \right) \cos\theta, \tag{25}$$

$$\frac{dv_z}{dt} = \frac{C_D \rho A}{2m} \left(v_x^2 + v_z^2 \right) \sin\theta - g,$$

$$\frac{dm}{dt} = -\frac{C_H \rho A}{2\zeta} \left(v_x^2 + v_z^2 - v_{CR}^2 \right) H(v - v_{CR}),$$

subject to the initial conditions

$$x(0) = 0, z(0) = z_0, m(0) = m_0, \tag{26}$$
$$v_x(0) = v_{x0}, v_z(0) = v_{z0}.$$

Equations (25) are solved subject to Equations (26), with default parameter values

C_D = 1 (dimensionless);
m = 10 kg;
g = 9.81 m/sec^2;
C_H = 0.10 (dimensionless);
ζ = 5.0x10^6 J/kg; and
v_{CR} = 3.0 km/s;

unless otherwise specified. The initial conditions (26) are consistent with a coordinate system at rest on the surface of the Earth directly beneath the interception point, with the intercept centre of momentum lying within the {xz} plane. Ignoring post-intercept Earth rotation, subsequent motion remains within the plane as no torques are present. Figure 4 shows schematic information flow in the re-entry simulation module.
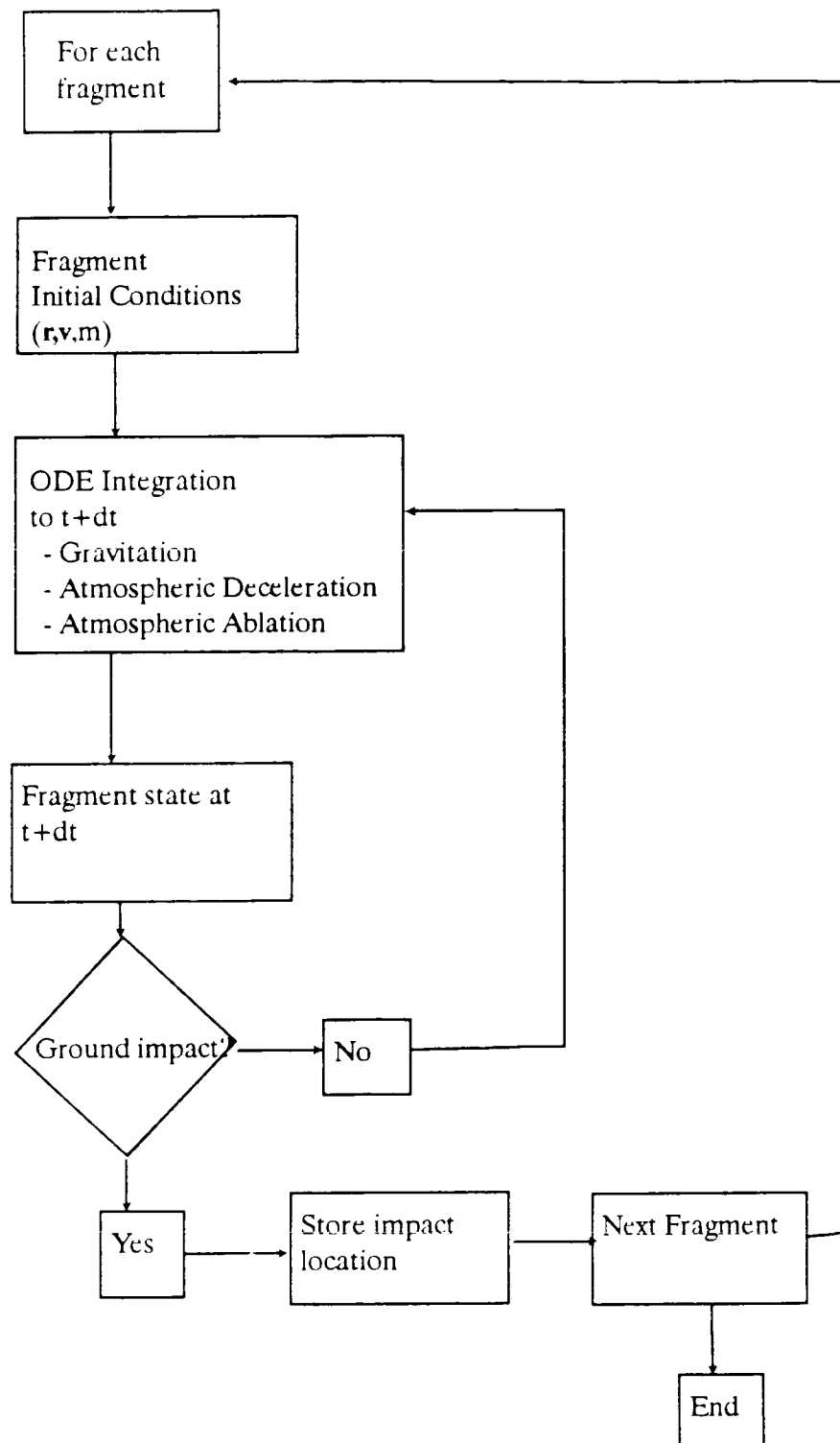
Figure 4: **Fragment Re-Entry Module -**
Conceptual Flow

NUMERICAL INTEGRATION TEST CASES

43. Equations (25) are numerically integrated using a fourth order Runge-Kutta integration scheme with adaptive stepsize control (Reference 24). The numerical integration package used has been validated and verified separately (Reference 17). The maximum estimated error tolerated during integration is $\varepsilon=1.0^{-6}$. The following paragraphs verify the re-entry simulation using progressively complex scenarios:

a.   vertical re-entry, no atmosphere;
b.   vertical re-entry, nonablative exponential atmosphere;
c.   vertical re-entry, ablative exponential atmosphere; and
d.   oblique re-entry, ablative exponential atmosphere.

Test Case 1: Vertical Re-Entry, Null Atmosphere

44. The Equations of Motion governing vertical re-entry in a vacuum are

$$\frac{d^2z}{dt^2} = -g, \quad z(0) = z_0, \quad v_z(0) = v_0, \tag{27}$$

with solution

$$v_z(t) = v_0 - gt, \quad z(t) = z_0 + v_0 t - \frac{1}{2}gt^2. \tag{28}$$

Figure 5 shows the results of numerical integration of these governing equations. Figure 5A shows altitude against time for initial re-entry speeds from 0 to 10 km/sec. Values are in agreement with Equation (31) to less than 10^{-3} fractional error. For example, descent from rest results in ground impact at time $t=(2z_0/g)^{1/2} = 142.8$ sec. Figure 5B shows velocity against time for reference bodies initially at rest and speed 1 km/sec, respectively. Least squares fits of the velocity profiles (using 100 data points) show them to be linear with a confidence of $r^2 = 1-10^{-8}$.
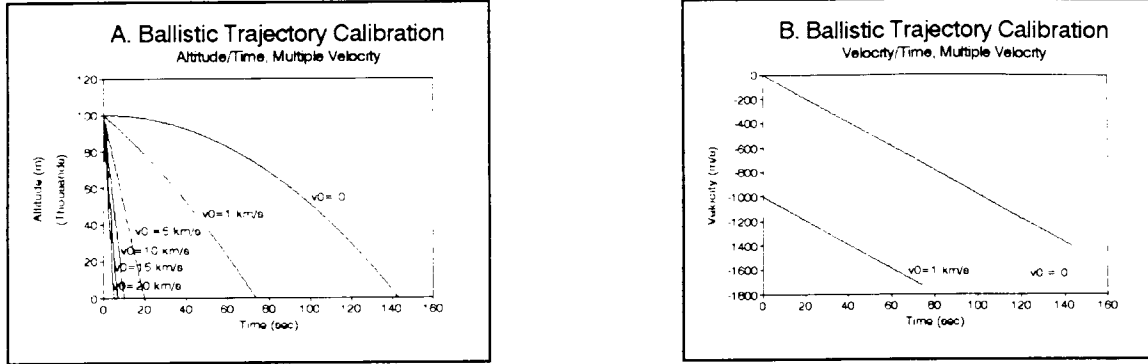
Figure 5: Ballistic Re-Entry Calibration Test 1: Vertical Re-Entry, Vacuum Approximation

Test Case 2: Vertical Re-Entry, Exponential Atmosphere

45. The analytical solution of the problem of vertical re-entry into an exponentially dense atmosphere has the form

$$v^2 = \exp\frac{\alpha}{\beta}(e^{-\beta h} - e^{-\beta z})v_0^2 - 2g\exp\left(-\frac{\alpha}{\beta}e^{-\beta z}\right)$$

$$\cdot\left\{(z-h) + \frac{\alpha}{\beta^2}(e^{-\beta h} - e^{-\beta z}) + \frac{\alpha^2}{4\beta^3}(e^{-2\beta h} - e^{-2\beta z}) + \frac{\alpha^3}{18\beta^4}(e^{-3\beta h} - e^{-3\beta z}) + ...\right\}. \tag{29}$$

Allan and Eggers (Reference 15) examined numerical and analytical solutions of this problem using a reference one-foot diameter iron sphere. Figure 6 repeats this analysis by way of verifying the atmospheric deceleration segment of the re-entry module. The figure assumes a 0.156 m (6 inch) radius iron sphere of mass 125.114 kg and 0.077 m^2 cross section, descending vertically from 60 km at an initial speed of 3.03 km/sec (10,000 ft/sec).

46. Figure 6 compares successively higher order approximations of the analytical infinite series with the numerical solution of the default test case. Figure 6A shows analytical and numerical re-entry velocity profiles including n=1-5 terms in the series.

Figure 6B is a detail for altitudes below one scale height. The presence of higher order terms increases the descent velocity at heights on the order of a single scale height ($z <$ 10 km). Visible in Figure 6A is the initial velocity increase of the test mass as it accelerates under gravity above the bulk of Earth's atmosphere. Significant atmospheric deceleration begins at about 40 km and continues until ground impact.
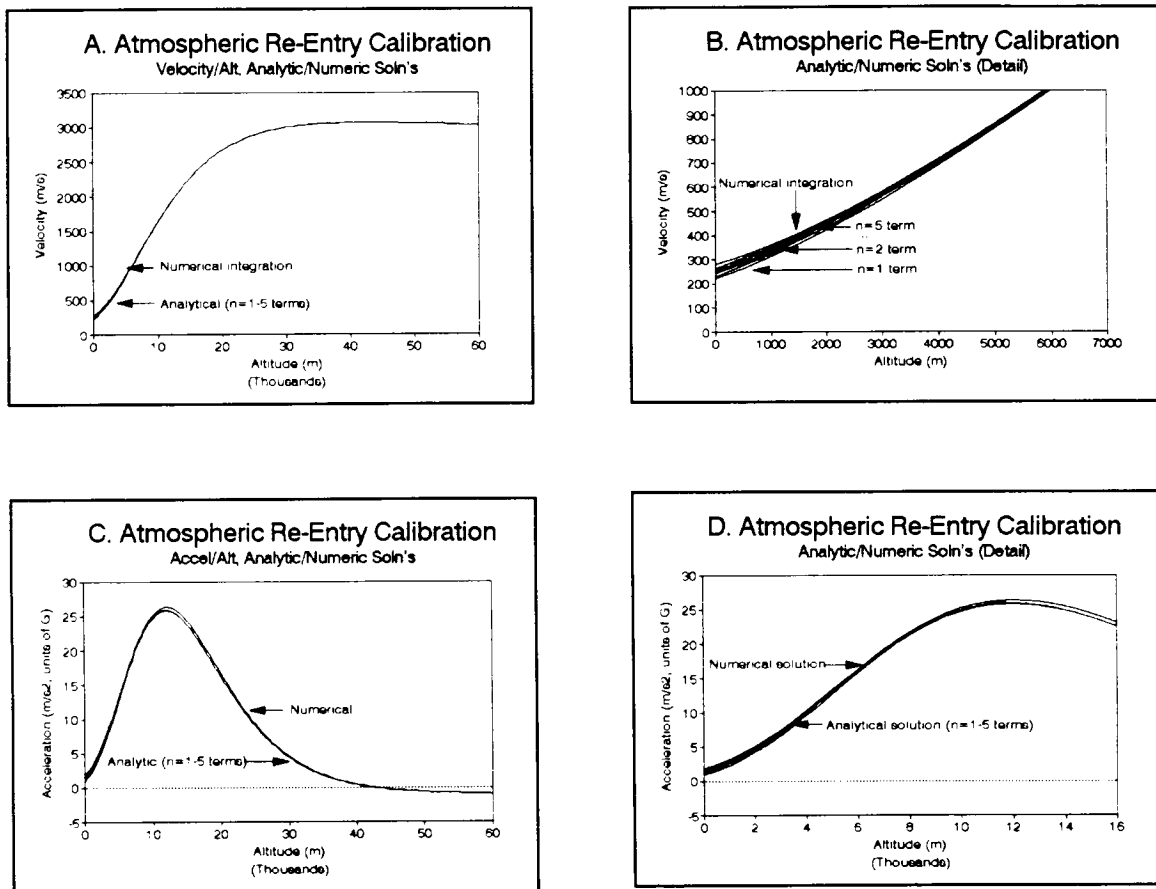

Figure 6: Ballistic Re-Entry Calibration Test 2:
Velocity and Acceleration Profiles with Atmospheric Deceleration

47.   Figure 6C compares the analytically approximated re-entry deceleration with that obtained numerically. High altitude acceleration is seen to be entirely due to gravity, up to an altitude of approximately 40 km. Atmospheric deceleration then dominates until ground impact, reaching a maximum value of approximately 26g at an altitude of about 12 km. The numerical and analytical solutions are seen to be in good agreement (Figure 6D): deviations are attributable to computational roundoff errors introduced during numerical differentiation.

48.   Figure 7 shows velocity with altitude during re-entry for initial velocities of the reference sphere from 1 km/sec through 15 km/sec. Speeds decrease markedly beginning near 40 km, with all impact speeds below 2 km/sec. Figure 7B shows the deceleration accompanying re-entry: atmospheric deceleration reaches almost 600g for the highest re-entry speed, with decelerations in excess of 400g occur for altitudes from 7-20 km. This deceleration is experienced for about one second at a average retarded speed of about 10 km/sec. The net effect of atmospheric deceleration is to dissipate approximately 99% of the initial projectile energy. Only 10 megajoules of the initial gigajoule kinetic energy accompanies impact: the remainder is dispersed in atmospheric and projectile heating. Figure 7 also verifies the result of Allen et al (Reference 15), that for a constant projectile type the altitude of maximum deceleration is independent of re-entry speed.
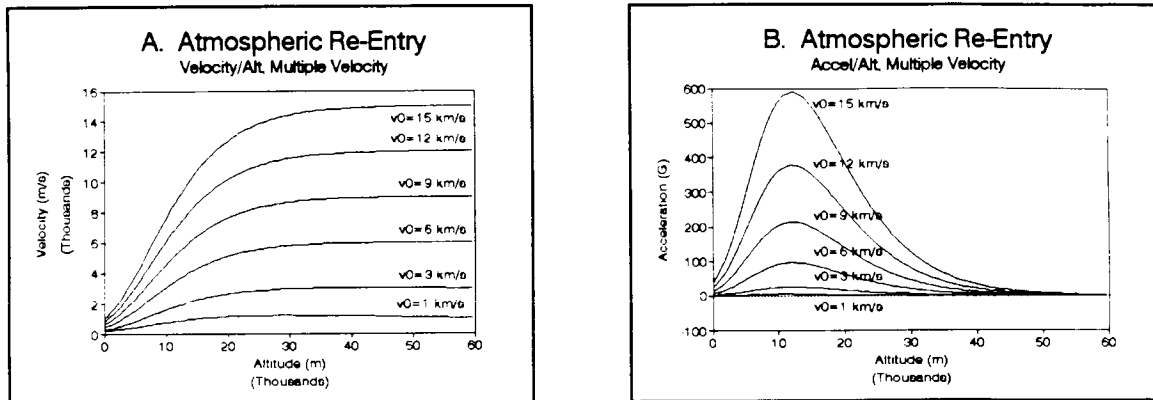
Figure 7: <u>**Velocity and Acceleration Profiles with Atmospheric Deceleration -**</u>
<u>**Constant Mass**</u>

49.   Figure 8 indicates the effect of the atmosphere's presence over a range of projectile masses. Spherical projectile masses from 0.01 kg through 1000 kg re-enter vertically with initial speed 3.03 km/sec. Figure 8A shows velocity profiles: lighter particles are more effectively decelerated by the less dense atmosphere at higher altitudes. Figure 8B shows deceleration profiles: the altitude and amplitude of greatest deceleration is a function of particle mass. Lighter particles are subject to less severe deceleration at higher altitudes than heavier masses.
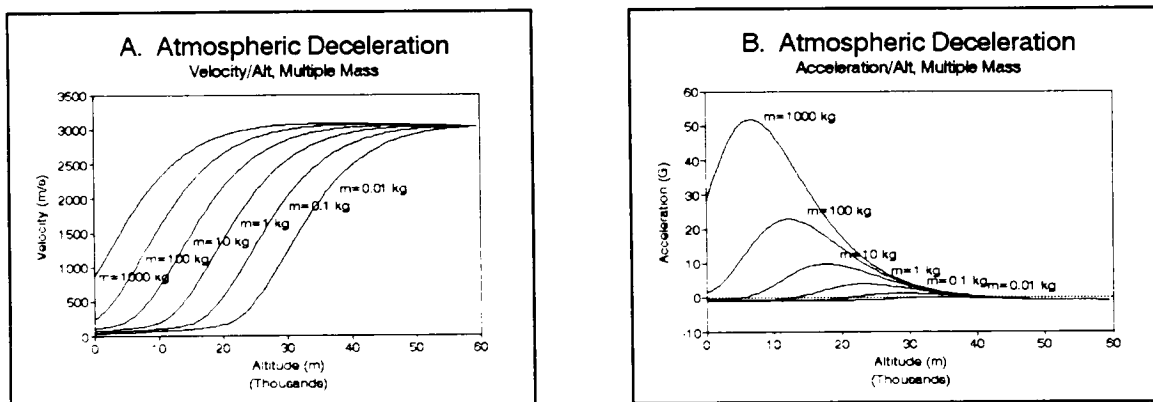
Figure 8: <u>**Velocity and Acceleration Profiles with Atmospheric Deceleration -**</u>
<u>**Variable Mass**</u>

Test Case 3: Vertical Re-Entry, Ablative Exponential Atmosphere

51.   Re-entry mass ablation occurs only while re-entry speed is above a critical threshold speed v_{CR}. For supercritical speeds, the mass ablation rate from Equation (10) is

$$\frac{dm}{dt} = -\frac{C_H \rho_0 A(m)}{2\zeta} e^{-\beta z} H\left(v^2 - v_{CR}^2\right), \tag{30}$$

with C_H the heat transfer coefficient (nominal default value 0.1), and ζ the heat of ablation (nominal default value 5×10^6 J/kg). Table 1 lists the total mass fraction lost during re-entry at speeds from three to 15 km/sec for the reference sphere. The table shows mass ablation to play a minor role in modifying re-entry behaviour for typical fragment compositions and re-entry speeds. Figure 7 shows projectiles to be rapidly decelerated to subcritical speeds while still at high altitude. Projectiles therefore travel through the densest and most erosive part of the atmosphere at subcritical speeds ($v_{Crit} = 3.0$ km/sec for the default fragment composition).

TABLE I: MASS FRACTION LOST DURING ABLATIVE ATMOSPHERIC RE-ENTRY

v_0 (km/sec)	$(m_0 - m_f)/m_0$
3.0	1.6×10^{-5}
6.0	4.08×10^{-5}
9.0	6.82×10^{-5}
12.0	9.66×10^{-5}
15.0	1.25×10^{-4}

Test Case 4: Oblique Re-Entry, Ablative Exponential Atmosphere

51.   Previous test cases have dealt only with vertical re-entry: this constraint is now relaxed as initial fragment velocities may lie anywhere within the reference {xz}-plane. Analytical solution of the governing Equations (9,10) remains possible but is no longer pedagogically useful. Figure 9 shows altitude/range profiles of a test mass during re-entry. Spherical test masses between 0.01 kg and 1000 kg are launched with initial velocity 5 km/sec depressed 22.5 degrees to the horizontal from an initial altitude of 100 km. Regardless of initial mass, trajectories are initially conic sections well approximated by straight lines, until the body experiences significant atmospheric deceleration beginning near 20 km altitude. Figure 9B is a low-altitude detail of Figure 9A: the increased efficiency of atmospheric deceleration with decreasing body mass is apparent.
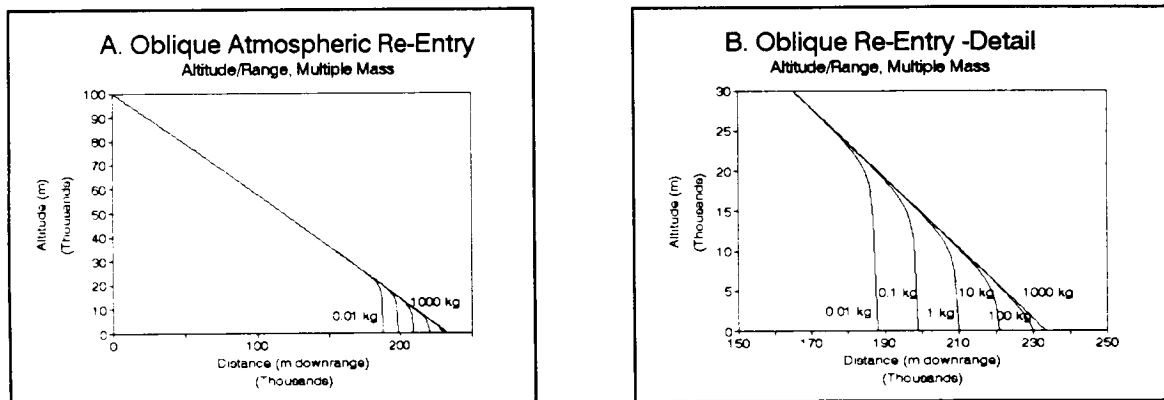

**Figure 9: Oblique Atmospheric Re-Entry Trajectories-
Variable Mass**

STREWN FIELD FORMATION

DEBRIS FIELD ANALYSIS

52.   The dynamic simulation segment models the ballistic re-entry of post-intercept fragments to produce the strewn debris field. This process can be repeated for each one-on-one engagement in a particular defence scenario to produce an ensemble of debris fields accompanying a specific launch corridor/defence site pairing.   This section addresses the subsequent analysis segment: the consolidation of the individual debris fields to produce a debris density map over the region of interest. This can be partitioned into two main sub-tasks:

1.   the determination of the fragment mass density of each strewn field; and
2.   the superposition of individual fields to produce a mean fragment mass density distribution.

Each sub-task is dealt with using simple analytic and geometric algorithms.

53.   The fragmentation module produces a set of N fragments with mass in the interval $[m_{min}, m_{max}]$. The set of N fragment impact sites form a possibly nonconvex polygon. The strewn debris field accompanying intercept is approximated by the convex hull of the impact N-gon, calculated using a simple box-wrapping algorithm (Reference 25). The post-intercept debris risk hazard is inferred through the size, shape and mean fragment density of the strewn field.

Sub-Task 1: Strewn Field Area

54.   To determine the mean fragment mass density associated with a strewn field it is required to find the field area. This is a polygon of n vertices on the Earth's surface (assumed spherical of radius a), denoted by $P_i = \{(\theta_i, \phi_i), i=1,...,n\}$. Let P_i be bounded by the minimal bounding rectangle $R_i = \{(\theta_i, \phi_i), \theta_{min} \leq \theta_i \leq \theta_{max}, \phi_{min} \leq \phi_i \leq \phi_{max}\}$. R_i is a subset

of a larger rectangular region R = {(Θ_{min},Θ_{max})x(Φ_{min},Φ_{max})} enclosing the entire region of interest.

55.   The area A_i of P_i is the double integral

$$A_i = \int_{P_i} a^2 d\sigma .$$
(31)

Denote the characteristic function of P_i as

$$\chi(\theta,\phi,P_i) = \begin{cases} 1, & (\theta,\phi) \in P_i , \\ 0, & (\theta,\phi) \notin P_i . \end{cases}$$
(32)

evaluated using an interior point checking algorithm (Reference 26). In terms of this the area becomes

$$A_i = a^2 \int_{\phi_{min}}^{\phi_{max}} \int_{\theta_{min}}^{\theta_{max}} \chi(\theta,\phi,P_i) \sin\theta \, d\theta d\phi ,$$
(33)

expressed as the Riemann sum

$$A_i = \lim_{\substack{\Delta\theta \to 0 \\ \Delta\phi \to 0}} \sum_{j=0}^{M} \sum_{k=0}^{N} a^2 \chi(\theta_j,\phi_k,P_i)\sin\theta_j \Delta\theta\Delta\phi .$$
(34)

where $\theta_j = \theta_{min}+j\Delta\theta$, $\phi_k = \phi_{min}+k\Delta\phi$. In practice the MxN mesh of Equation (34) remains finite though small, allowing the approximation

$$\check{A}(\Delta\theta,\Delta\phi,P_i) = \sum_{j=0}^{M} \sum_{i=0}^{N} a^2 \chi(\theta_j,\phi_i,P_i)\sin\theta\Delta\theta\Delta\phi .$$
(35)

An exactly computable example appears below.

56.   Having approximated the field area to a desired precision, the mean fragment mass density follows as

$$\rho_i = \frac{M_{RV} + M_{IV}}{A_i}, \qquad (36)$$

(M_{RV}, M_{IV}) the re-entry and intercept vehicle masses, respectively. This assumes for simplicity a zeroth-order variation in debris density: the debris is distributed uniformly across the entire field.

Example: Area of Rectangular Region of Unit Sphere

57.   Consider the rectangular region bounded by the latitude/ longitude pairs:

$$\{(30°N,30°W), (30°N,60°W), (60°N,60°W), (60°N,30°W)\}.$$

on the surface of the unit sphere. The surface area is evaluated as

$$A = \int_{\pi/6}^{\pi/3} d\phi \int_{\pi/6}^{\pi/3} \sin\theta \, d\theta$$
$$= \frac{\sqrt{3}-1}{12} \pi \qquad (37)$$
$$= 0.19165...$$

Table II shows the approximate area for several mesh sizes using the double sum Equation (37).

TABLE II:
APPROXIMATION OF DEMONSTRATION AREA INTEGRAL

Mesh (deg)	A~	Abs(A~-A)/A
(1.0,1.0)	0.19039	0.007
(0.5,0.5)	0.19102	0.003
(0.25,0.25)	0.19134	0.001
(0.125,0.125)	0.19149	0.0008
(0.0625,0.0625)	0.19157	0.0004

Sub-Task 2: Ensemble Field Superposition

58.   Sub-task 2 evaluates the mean strewn debris density by summing over all one-on-one engagements within a particular scenario. The mean density at a location (θ,ϕ) summed over all S engagements is

$$<\rho(\theta,\phi)> = \frac{1}{S}\sum_{i=1}^{S}\rho_i(\theta,\phi) \tag{38}$$

This is most easily computed by binning results over the region of interest R. Let R be divided into bins of size $\{a\Delta\theta, a\Delta\phi\}$ on a sphere of radius a, forming a mxn mesh. The field P_i has a matrix representation

$$D_i = \begin{pmatrix} 0 & 0 & 0 \\ 0 & \rho_i U^i & 0 \\ 0 & 0 & 0 \end{pmatrix} \tag{39}$$

with

$$U_{jk}^i = \chi(\theta_j,\phi_k,P_i) . \tag{40}$$

This is summed over all S intercepts to form the mean density matrix

$$D = \frac{1}{S}\sum_{i=1}^{S} D_i , \tag{41}$$

where

$$D_{jk} = \frac{1}{S}\sum_{i=1}^{S} \rho_i\chi(\theta_j,\phi_k,P_i) . \tag{42}$$

This procedure is implemented to determine the approximate area and mean fragment density for individual and multiple strewn fields. Information flow for the strewn field module is shown in Figure 10.

```
┌─────────────────┐
│ For each        │
│ impact location │
└─────────────────┘
        │
        ▼
┌─────────────────┐
│ Generate bounding│
│ polygon         │
└─────────────────┘
        │
        ▼
┌─────────────────┐
│ Find Convex Hull│
└─────────────────┘
        │
        ▼
┌─────────────────┐
│ Find Hull       │
│ Area            │
└─────────────────┘
        │
        ▼
┌─────────────────┐
│ Find mean       │
│ fragment        │
│ mass density    │
└─────────────────┘
```
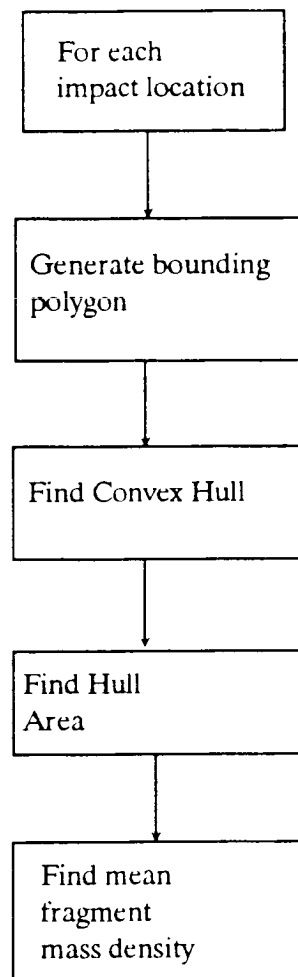
Figure 10: Strewn Field Module -
Conceptual Flow

MODULE INTEGRATION

59.   The previous section documented the fragmentation, re-entry and strewn field modules comprising the strewn field simulation. This section extends that to examine each module's integration into the overall simulation. Specifically, we examine:

a.   fragmentation/re-entry module integration; and
b.   re-entry/strewn field module integration.

The first section describes the integration of the fragmentation and fragment re-entry modules, showing fragment trajectories accompanying a variety of re-entry conditions. The second section discusses integration of the fragment and strewn field modules, using graphics packages to introduce the effect of re-entry conditions upon strewn fields.

STANDARD PARAMETER VALUES

60.   Each simulation module is based on a hierarchical architecture: complex simulation elements are progressively combined from simpler sub-elements. Ultimately each sub-element consists of a set of descriptors, which may be either static or dynamic throughout the simulation. This section lists the static descriptors forming the standard parameter set.

61.   The default Interceptor Vehicle (IV) static parameter values are:

a.   Mass = 10 kg;
b.   Mean material density = 7900 kg/m^3.[5]

All additional IV descriptors are dynamic position and velocity records. The default Re-entry Vehicle (RV) static parameter values are:

c.   Mass = 1000 kg;

---

[5]   Assumed stainless steel fragment material (Reference 22). Construction materials may be freely varied. This value and material is for demonstration purposes only.

d.   Mean material density = 7900 kg/m^3.

All additional RV descriptors are dynamic position and velocity records.

62.   The default fragmentation process consists of forming 4x32 = 128 fragments of mass 100 gm, 1 kg, 10 kg, 100 kg. Fragments of mass less than 100 gm will remain aloft sufficiently long that prevailing winds will play a significant role in their eventual dispersion; fragments larger than 10% the original RV mass are unlikely to survive hypervelocity impact. Fragment mass density is assumed equal to the RV/IV density. Ballistic parameters governing fragment ejection and re-entry are discussed below.

FRAGMENTATION/RE-ENTRY INTEGRATION

63.   The fragmentation and atmospheric re-entry modules are integrated as follows: initial conditions for the fragmentation module are provided as Re-entry Vehicle/Intercept Vehicle (RV/IV) position and velocity with respect to inertial geocentric equatorial coordinates.[6] The RV and IV mass and composition are fixed parameters throughout each simulation run. The fragmentation module simulates collisionally generated fragments ejected with a range of initial masses. Ejection speed is found using the mass/velocity distribution Equation (2) for each sample mass, and ejection is assumed to be spherically symmetric in the RV/IV centre of mass (CM) coordinate frame (Reference 28). Unless otherwise mentioned, multiple fragment clusters are ejected azimuthally uniformly at 45° elevation. This gives maximum range trajectories, resulting in the maximal strewn field extent. The fragmentation module converts each fragment velocity from RV/IV CM coordinates to inertial geocentric equatorial position and velocity vectors.

64.   The atmospheric re-entry module accepts as initial conditions inertial fragment position and velocity vectors. For altitudes above 100 km, ballistic motion is simulated

---

[6]   The inertial geocentric equatorial coordinate system (or xyz system) has origin at the Earth's centre, z-axis aligned with the Earth's rotation vector, x-axis pointing towards vernal equinox through the equator, and y-axis passing through the equator at 90°E to form a right-handed coordinate system (References 16,27). As the Earth rotates, the longitude of the x and y axes drift westward at 360°/24 hr = 15°/hr.

using a satellite orbital motion generator (Reference 1,27). At 100 km altitude, fragment state vectors are converted from geocentric equatorial inertial coordinates to topographic horizon coordinates for an observer directly below the fragment.[7] If intercept occurs below 100 km altitude, the conversion to topographic horizon coordinates is immediate. For each fragment, initial conditions are passed to the numerical integration package and the subsequent trajectory followed to ground impact.

65.   The following figures show fragment trajectories resulting from a variety of intercept conditions. The default intercept conditions are:

   a.   RV mass 100 kg, velocity 5 km/sec (south);
   b.   IV mass 100 kg, velocity 5 km/sec (north);
   c.   Intercept altitude 20 km; and
   d.   Ten fragments with mass 0.1 kg each, ejected in the vertical (South/Up) plane.

Parameter values are chosen to demonstrate module integration, and should not be construed as representing actual ballistic missile intercepts.

66.   Several cases are presented:

   a.   Default intercept, zero momentum;
   b.   Zero momentum, low velocity;
   c.   Zero momentum, low altitude;
   d.   Tangential momentum;
   e.   Oblique momentum;
   f.   Nominal RV/IV masses.

Parameter values are selected by computer operating system limitations: the graphics package can only accommodate ten open trajectory files, while memory constraints require relatively low-altitude intercepts. Neither constraint affects the final simulation package.

---

[7]   The topocentric horizon (or SEZ) coordinate system associated with an observer P has origin at rest on the surface of the Earth at the observer's position. Axes are conventionally taken to be in the south, east and up directions. The coordinate system must be defined with respect to a specific observer (References 16,27). Conversion utilities between SEZ and xyz coordinates are documented at Reference 27.

Case 1: Default Parameters

67.   Figure 11 shows fragment trajectories produced using the default parameter settings. Individual trajectories are visible as dotted lines indicating position at one-second intervals. IV and RV mass and velocity have been chosen to yield zero net momentum: this is for pedagogic purposes to demonstrate the initially spherically symmetric fragmentation pattern. Spherical symmetry is broken by atmospheric and gravitational forces. Figure 11 shows fragments ejected downwards being rapidly decelerated by the increasingly dense atmosphere, while particles ejected upwards are little hindered by atmospheric damping. The 100 gm fragments used in Figure 11 reach a maximum altitude in excess of 150 km, and a maximum range of more than 175 km. The area of the strewn debris footprint is approximately 100,000 km^2; assuming debris to be uniformly scattered within the region gives a mean fragment mass density of 2 gm/km^2, or one 100 gm fragment per 100 km^2.
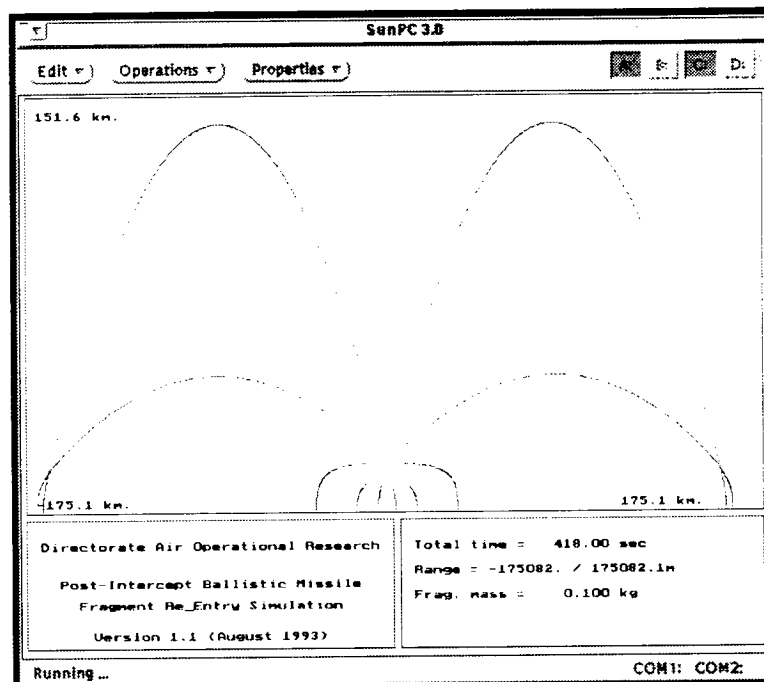
**Figure 11:   Fragmentation/Re-Entry Trajectories:
Default Configuration**

Case 2: Zero Momentum, Reduced Velocity

68. Figure 12 demonstrates the effect of reduced interception velocity upon fragment re-entry trajectories. In this scenario RV and IV velocities have been reduced from 5 km/sec to 2.5 km/sec, diminishing the total kinetic energy available for fragmentation and ejection by a factor of 4. Particles now reach a greatest height of only 33.2 km (13.2 km above the intercept point), reduced by a factor of 10 from the default case. The maximum ejecta range is now 26.8 km, reduced from 175.1 km. This reduction by a factor of about 6 results in a reduction by a factor of 36 in strewn debris field size and a corresponding increase in fragment density.
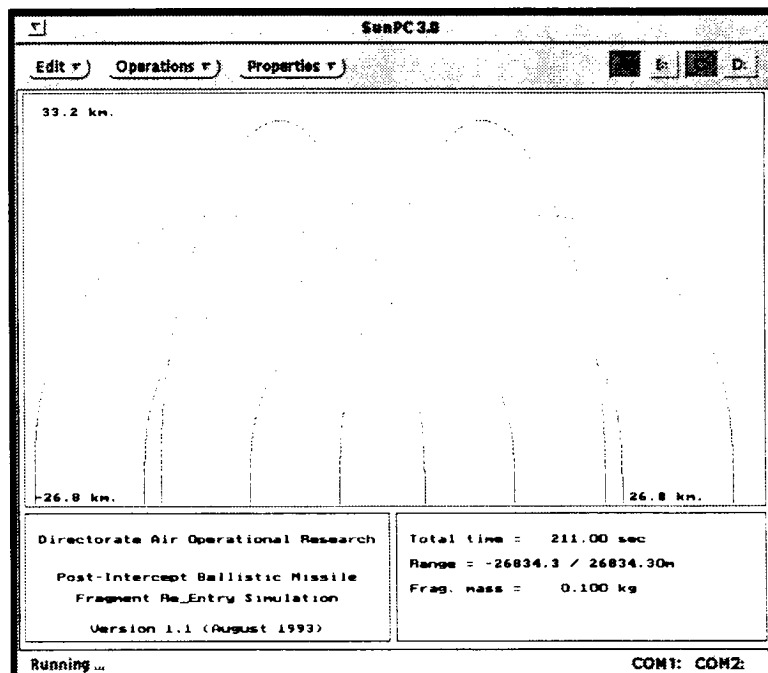
Figure 12: Fragment Trajectories: Reduced Velocity

Case 3: Zero Momentum, Reduced Altitude

69.   Figure 13 shows the fragment pattern resulting from the default intercept occurring at 10 km altitude. Reducing intercept altitude from 20 km to 10 km increases the atmospheric density by a factor of 4. Fragment kinetic energy is transferred to the atmosphere through deceleration and heating more efficiently, resulting in reduced fragment altitude and range.

Figure 13: <u>Fragment Trajectories: Reduced Altitude</u>

Case 4: Tangential Momentum

70.   Previous figures have shown zero-momentum intercepts. The intercept of Figure 14 has a net tangential momentum in the direction of the re-entry 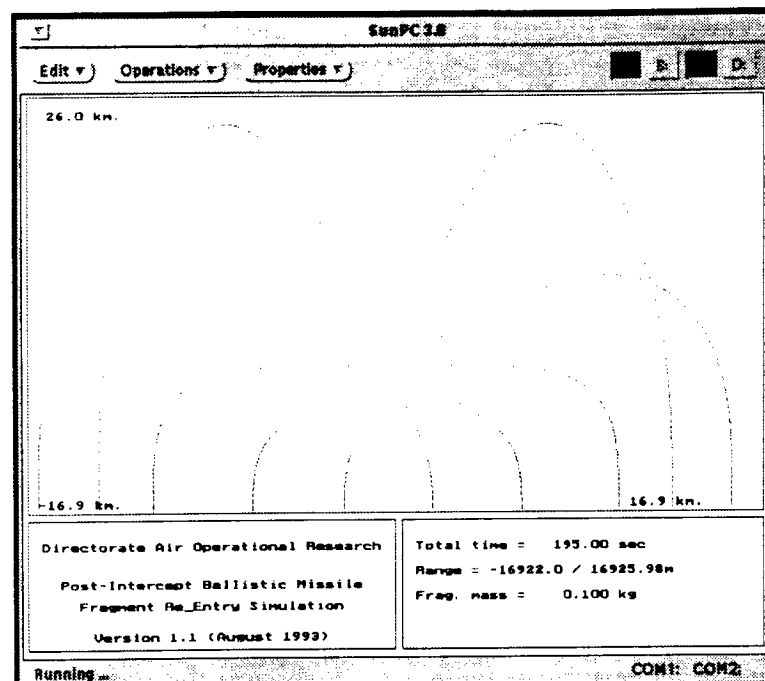vehicle (page right). Collision has occurred between two bodies of equal mass with velocity 5 km/sec (south) and 1 km/sec (north). The initial fragment distribution is no longer spherically symmetric, but skewed along the direction of net momentum. Fragments are initially distributed along a cone with its symmetry axis along the direction of momentum. Fragments propagated initially downwards are rapidly decelerated, while those propagated upwards have greater range by virtue of both elevated trajectory and less dense atmosphere at higher altitudes. The net effect upon the strewn debris field is to shift the field away from the intercept point. Subsequently the field will be shown to be elliptical or ovoid.
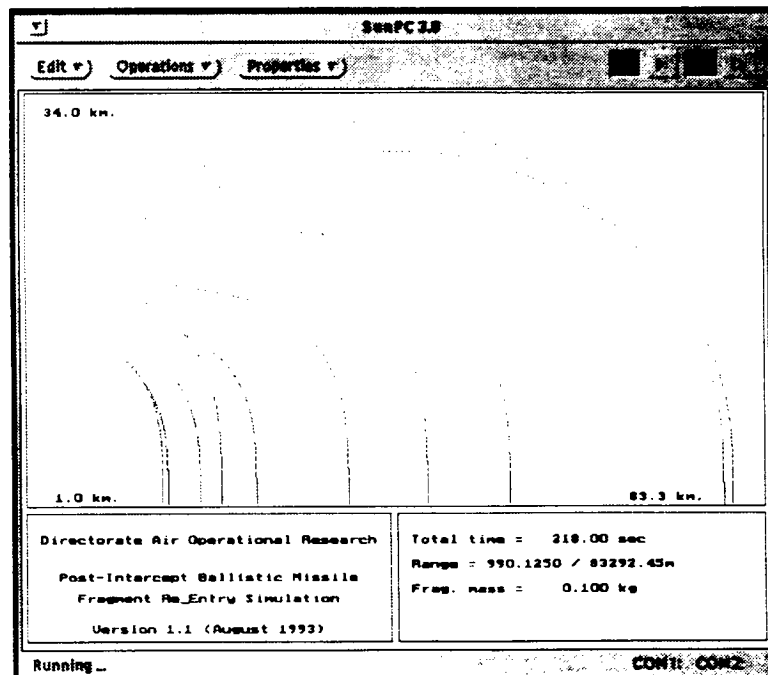
Figure 14: <u>Re-Entry Trajectories: Tangential Momentum</u>

Case 5: Oblique Momentum

71. Figure 15 shows fragment trajectories resulting from an oblique collision: the default RV travelling 5 km/sec (south) has been intercepted by the default IV travelling at 5 km/sec (up). Net momentum is directed south-up at 45°, upwards to the right. The comments of Case 4 remain applicable: the strewn field occurs downrange of the intercept point.
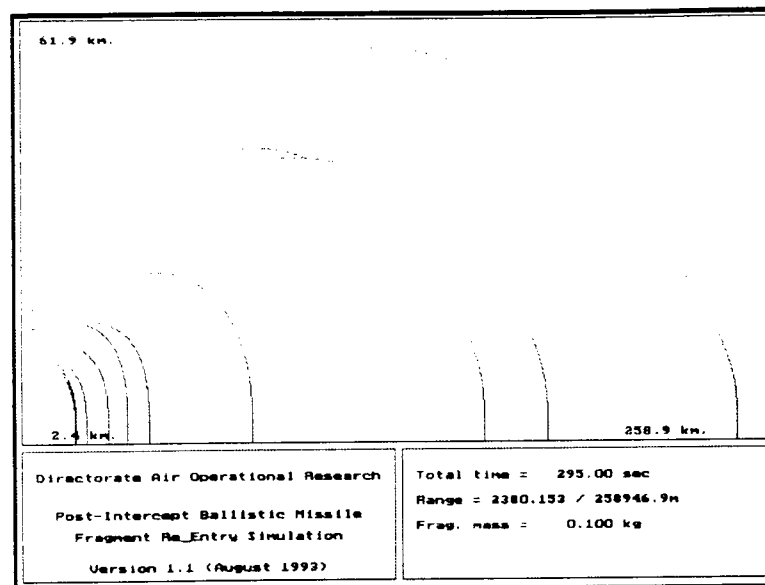
Figure 15: Re-Entry Trajectories: Oblique Momentum

Case 6: Nominal RV/IV Masses

72.   Figure 16 indicates trajectory profiles accompanying nominal RV and IV masses. Default RV mass of 1000 kg and RV mass of 10 kg are shown. Both particles travel horizontally with 5 km/sec velocity. RV motion is to page right, IV motion to page left. The net momentum is in the RV direction of motion.   At constant velocity, net momentum is to the right: RV momentum is diminished by 1 per cent following interception.

Figure 16: <u>Re-Entry Trajectories, Reference RV/IV Masses</u>

Case 7: Tangential Momentum Intercept, Multiple Fragment Mass

73.   Adding trajectories from fragments with a range of masses introduces an additional degree of complexity to the re-entry module. Figure 17 shows Case 4 (nonzero tangential momentum) with fragments of mass 0.1 kg and 10 kg. One hundred gram fragments are ejected with a speed of 978.88 m/sec with respect to the RV/IV CM, while ten kilogram fragments are ejected at 193.40 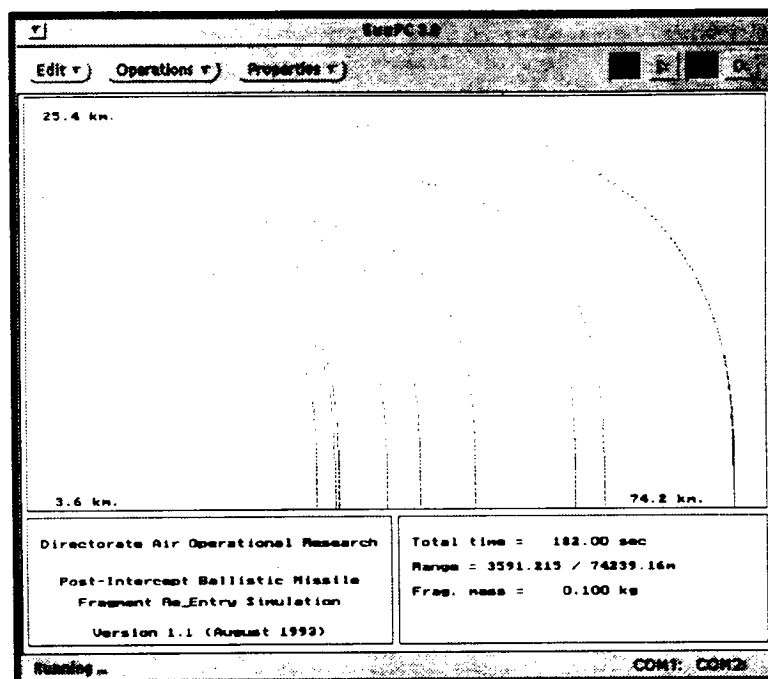m/sec for this collision. Interception occurs at 20 km altitude, approximately three atmospheric scale heights. The two mass classes can be distinguished by their differing initial ejection speeds. Fragment trajectories, and the eventual strewn field dispersion pattern, are determined primarily by two processes: ejection speed and fragment mass. Heavier fragments are ejected at slower speeds than lighter fragments, but are less affected by atmospheric drag.

74.   The competition between these two processes can be seen in the following figures. In Figure 17, consider 0.1 kg and 10 kg fragments ejected upwards. The 0.1 kg fragment is more affected by atmospheric deceleration, but at higher altitudes the net effect is still insufficient to offset the fragment's higher ejection speed. The lighter fragment impacts further downrange than the heavier fragment. Contrast this with the two fragments ejected *downwards* in Figure 17. Both 0.1 kg and 10 kg fragments are propelled at different speeds into the increasingly dense atmosphere: the 0.1 kg fragment is more efficiently decelerated than the 10 kg mass, resulting in the lighter fragment landing further uprange than the heavier fragment. The net effect on the strewn field distribution is to produce the heavier fragment field within the lighter fragment field, in a 'bullseye' pattern.
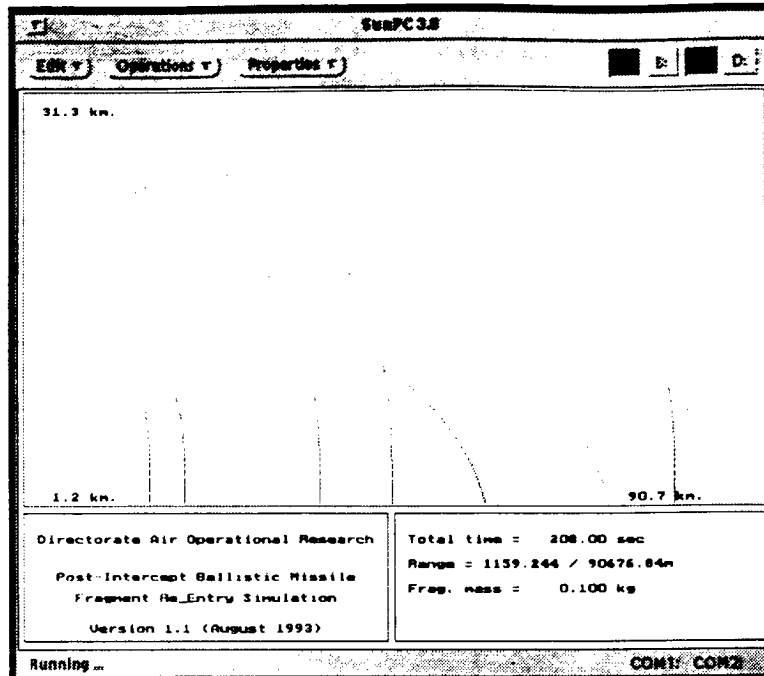
Figure 17: <u>Re-Entry Trajectories, Default Case,</u>
<u>Multiple Fragment Masses</u>

Case 8: Reduced Altitude, Multiple Fragment Masses

75.   Figure 18 repeats the intercept of Case 7 with the altitude reduced from 20 km to 10 km. The effect of increased atmospheric density is visible: lighter fragments are more efficiently decelerated than heavier fragments, and heavier fragments impact further downrange. The ground dispersion pattern is now fundamentally different from that of Case 7: the bullseye pattern has been replaced by one with heavier fragments extending downrange beyond the light fragment field.
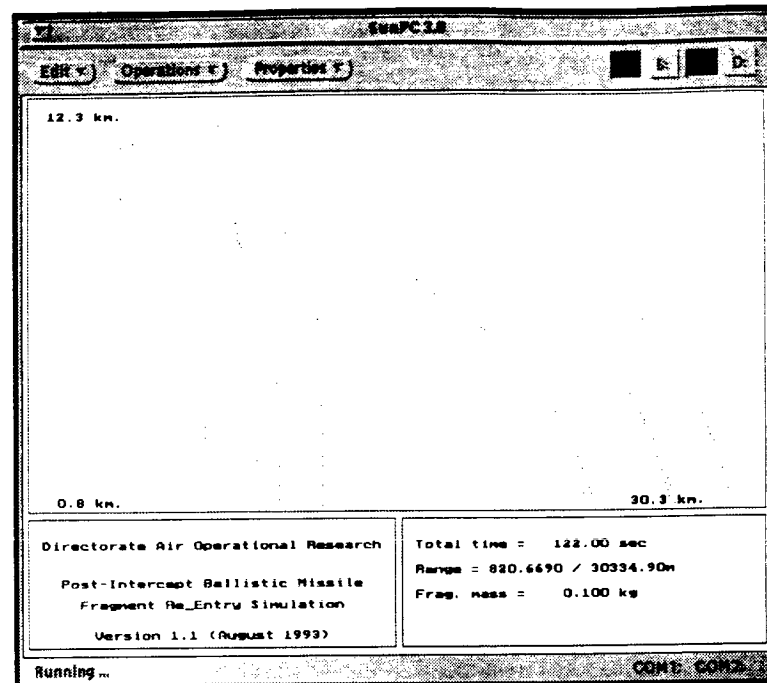
Figure 18: **Re-Entry Trajectories, Decreased Elevation,**
Multiple Fragment Masses

STREWN FIELD ANALYSIS

76. The fragment re-entry module concludes with the impact of fragments to form a strewn debris field. Figures 19 and 20 illustrate two strewn fields resulting from zero momentum and tangential momentum collisions, respectively. Interception takes place over Labrador (55°N, 60°W) at an altitude of 1000 km, with the RV travelling west at approximately 5 km/sec. Intercept data was derived from the program *BMKILL*, documented separately (Reference 2). Strewn fields were produced by the *Pascal* computer program *SDF_PC*, documented in the following section.

77. Figure 19 shows the strewn fragment field resulting from a zero momentum collision (RV and IV masses equal, equal and opposite velocity). Fragments of mass 0.1,

1, 10, 100 kg are shown, with line segments connecting fragments of equal mass. Fragments of equal mass are ejected with spherical symmetry in the CM frame, with lighter fragments ejected at higher speeds, producing the bullseye pattern. Heavy fragments impact near the centre of the bullseye; lighter fragments impact over a wider region.
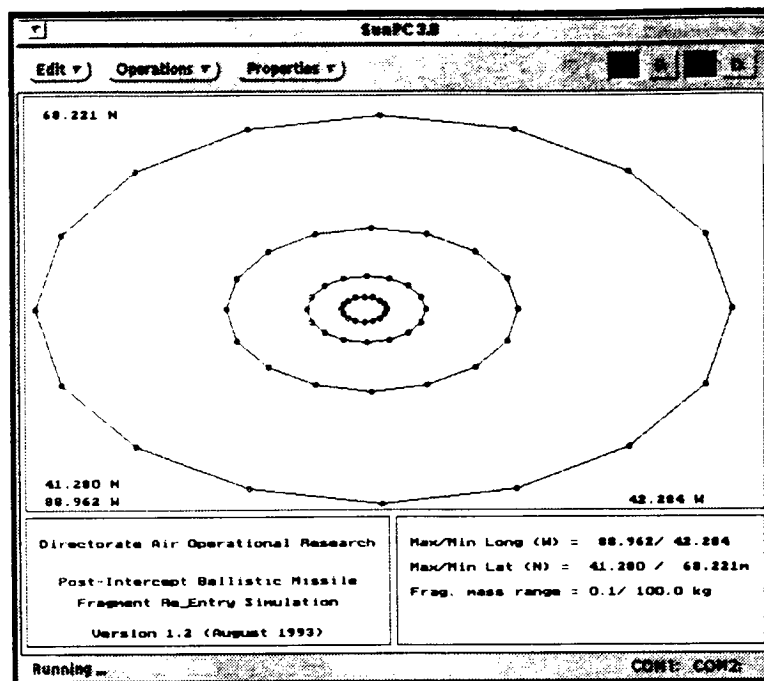
Figure 19: <u>Strewn Debris Field, Zero Momentum Case</u>

78.   Figure 20 shows the strewn field resulting from the same interception, but now with 10 kg IV and 1000 kg RV masses. Net momentum is tangent to the RV trajectory to the west (page left). Fragment ejection is no longer spherically symmetric, but takes place along the surface of a cone opening in the direction of momentum. Fragments enter the atmosphere obliquely, with lighter fragments preferentially decelerated, resulting in the non-concentric fragment pattern.
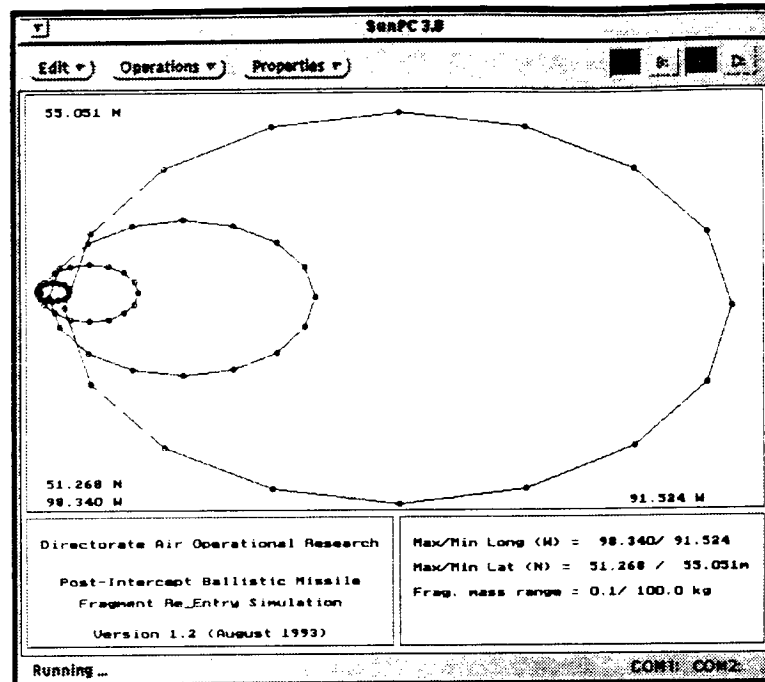
Figure 20: <u>**Strewn Debris Field, Tangential Momentum**</u>

III. IMPLEMENTATION

INTRODUCTION

79.   This section describes the computer implementation of the processes discussed above. The primary analysis tool is the Strewn Debris Field Simulator *SDF_SIM:* this package is written in the Pascal programming language using Borland's *Turbo Pascal Version 6.0* for PC platforms (Reference 29) using accepted simulation standards and procedures (Reference 30). SDF_SIM accepts as input intercept data provided by BMDKILL (Reference 2). Fragmentation, re-entry and field deposition are modelled using the previous section's procedures. SDF_SIM produces as output a debris file containing the convex hull of the strewn field, as well as a listing of all impact points. A second version of SDF_SIM, *CSDF_SIM*, produces the composite strewn debris field produced by multiple ballistic missile intercepts. CSDF_SIM has been adapted to run on a SUN workstation under UNIX. Strewn field analysis is performed by a post-processor program, providing graphics displays of intercept data. SDF_VIEW displays individual and composite strewn fields. The implementation and use of each of these tools is discussed below.

USER'S GUIDE

SDF_SIM

80.   SDF_SIM requires little user interface: input files are handed over from BMDKILL or an equivalent package. Debris fields are created and stored automatically. The default input file consists of a set of missile intercept records. Record structure is

shown in the example below. The missile intercept record producing the strewn field of Figure 19 is:[8]

```
 47.58   -97.25  BM target coords (deg N, E)
20.91951342  Time since BM launch that intercept occurs (min)
 54.75   297.84  1015.26  Lat Long and Alt(km) of intercept
0.36504197  -0.56067317  0.94661696  Intercept position vector (du)
-0.58519845  -0.32571664  -0.17582570  BM vel vector at intercept (du/tu)
0.13758965  0.23717267  0.58611500  ABM vel vector at intercept (du/tu)
```

All field values are produced automatically by BMDKILL. Position and velocity measurements are in equatorial geocentric inertial coordinates and measured in canonical units: 1du (distance unit) is one mean Earth radius (6378.137 km (WGS84, Reference 17)), 1 du/tu is the speed of a circular orbit with radius 1 du (7.905368 km/sec, Reference 16).

81.   SDF_SIM is currently configured to accept intercept files labelled RUNnn. The screen dialog below shows the processing the file RUN1 containing a single intercept (user entries in bold):

```
C:\DEBRIS> SDF_SIM
        Run Number?
        1

        Intercept #1....
        Simulation complete!

C:\DEBRIS>
```

The convex hull is directed to the file D_1_1.HUL (Debris pattern for File = RUN1, Intercept = 1), and the set of impact points to D_1_1.TOT. The first line of the hull file contains the number of points forming the convex hull, as well as the total number of fragments modelled. The remaining rows contain longitude (deg E) and latitude (deg N) values for each impact point in the hull:

---

8   All missile launches, interceptions and fragmentations are entirely for demonstration purposes only.

18 64

264.93135	51.26819
266.18305	51.41190
267.24417	51.82172
267.95313	52.43528
268.46422	53.28865
268.47612	53.32326
268.46420	53.35787
267.95272	53.88311
267.24343	54.49683
266.18208	54.90688
264.93031	55.05084
263.67870	54.90686
262.61777	54.49690
261.90901	53.88341
261.66026	53.15977
261.90940	52.43609
262.61851	51.82250
263.67966	51.41239

The TOT file consists solely of lat/long pairs and will not be presented. Run times using default parameters and 4x16=64 fragments are on the order of 10 minutes per interception using a 486DX.

CSDF_SIM: Structure and Use

82.   CSDF_SIM computes composite strewn debris fields accompanying multiple interceptions. Functionally, CSDF_SIM is identical to SDF_SIM with an additional DO UNTIL EOF loop to increment records. Structurally, additional file management routines are provided because of increased housekeeping requirements. CSDF_SIM has been ported to SUN workstations to take advantage of greater speed and throughput under UNIX. Run time is reduced from about 10 minutes per record (486DX) to less than 90 seconds (SUN ET4). In usage, CSDF_SIM is identical to SDF_SIM with one exception: multiple run files can be examined by using the metafile MASTER.LST, which contains a list of all intercept files to be processed.

SDF_VIEW

83.   SDF_VIEW is a post-processor program which displays strewn debris fields produced by SDF_PLOT and CSDF_PLOT. The package uses Pascal's screen graphics utilities: screen images can subsequently be captured, for example using WordPerfect's GRAB utility. A user

dialog to create an orthographic map of North America with the strewn field of RUN1 appears below:

C:\DEBRIS>**SDF_PLOT**

Specify type of map projection:
            (1) Orthographic
            (2) Mercator
            (3) Polar
              1

Which of the following maps would you like to display?
            (1) N. America
            (2) S. America
            (3) Europe
            (4) Africa
            (5) Asia
            (6) Australia
            (7) Antarctica

              1

Default Central Lat and Long of the map projection is:
        Lat = 60.00 degrees N.
        Long = 260.00 degrees E.

Accept these defaults? (y/n) **y**

How many data sets to overlay on this map? **1**

Filename for data set # 1? **d_1_1.hul**

Shade in this contour? (y/n) **y**

========= Select Contour Shading and Color ========

Select the filling pattern:

        (1)   Solid
        (2)   Lines
        (3)   Thin slashes
        (4)   Thick slashes
        (5)   Thick Backslashes
        (6)   Thin Backslashes
        (7)   Thin hatched
        (8)   Heavy cross hatch
        (9)   Interleaving lines

(10) Wide spaced dots
(11) Close spaced dots
   10

========= Select Contour Shading and Color ========

Select the pattern color:
   (0) Black
   (1) Blue
   (2) Green
   (3) Cyan
   (4) Red
   (5) Magenta
   (6) Brown
   (7) Lt Grey
   (8) Dk Grey
   (9) Lt Blue
   (10) Lt Green
   (11) Lt Cyan
   (12) Lt Red
   (13) Lt Magenta
   (14) Yellow
   (15) White

   14

Plot Canadian cities? (y/n) **y**

Plot ground based radar site(s)? (y/n) **y**

Current default positions for GBRs:

N. Latitude   E. Longitude
   47.57   262.75

Accept these defaults? (y/n) y

Plot ground based interceptor site(s)? (y/n) **y**

Current default positions for ABM sites:

N. Latitude   E. Longitude
   47.57   262.75

Accept these defaults? (y/n) y

The screen display resulting from these input parameters appears in Figure 21.
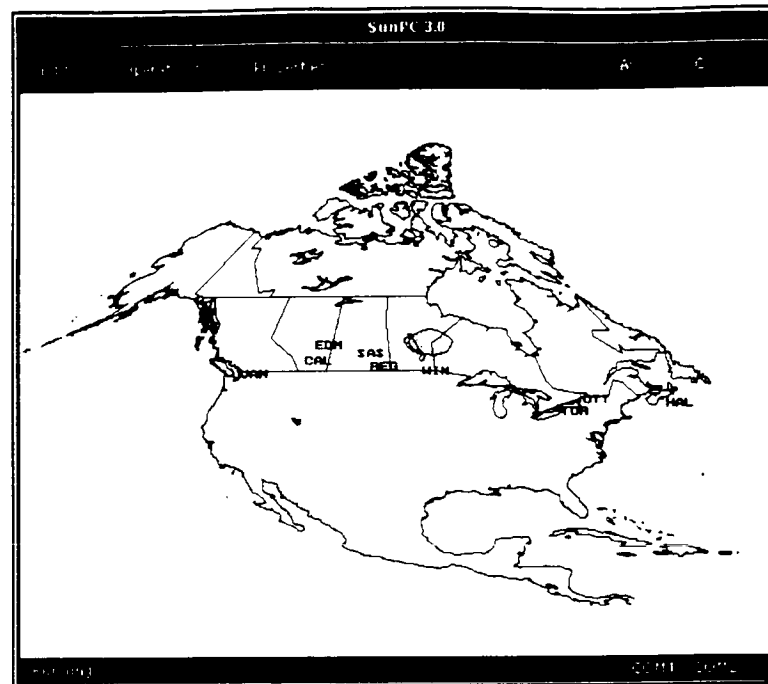
Figure 21: <u>SDF_VIEW: Strewn Debris Field Display</u>

V. DISCUSSION

84.   This section identifies opportunities for further development of the strewn debris field model. There are three principal areas for advancement:

Area A: Improve the fidelity of the existing system;
Area B: Expand the scope of the existing system; and
Area C: Improve the interoperability of the existing system.

For each of these areas, there area two avenues for improvement, which we will denote by Type 1 and Type 2:

Type 1:   Technical improvement through increased computer resources, more careful design and greater data throughput; and
Type 2:   Conceptual improvement through incorporation of additional theoretical and experimental understanding.

Implementing Type 1 or 2 improvements to any of Areas A-C represents an increase in model fidelity at the cost of added complexity. The following paragraphs discuss a few of the cost/benefit issues associated with each.

INCREASED FIDELITY

85.   The fidelity of the current system can be improved by using more accurate models of the processes simulated. Each of the fragmentation, re-entry and strewn field modules can be enhanced to provide more accurate results, although not all in the same manner. Type 1 improvements to the fragmentation model would yield more data by increasing production, but not necessarily provide a better understanding.

86.   Significant improvements to the fragmentation module must come from Type 2 improvement; better understanding of the physics of hypervelocity impact. The current literature contains relatively little of the mass, number and velocity distributions of collisionally generated fragments. What information is available has been obtained over a comparatively narrow range of impact energies: these results must be scaled to extend these relationships to the hypervelocity

regime. There is much opportunity for work in both the theoretical and experimental understanding of hypervelocity physics. Enlarging this information data base will do much to improve the first-order and necessarily tentative results presented herein.

87.   The physics of atmospheric re-entry has evolved rapidly over the past few decades, with much experience being collected and organized, so that the process is now well-understood (for example, Reference 19, and references cited therein). This database can be added to the re-entry module as necessary, perhaps to model fragment or warhead heating using a fluid dynamic approach based on the Navier-Stokes equations (Reference 31). The primary avenue for improving the re-entry module is through Type 1 enhancement: the numerical integration code can be streamlined to reduce program runtime or the code can be expanded to accommodate nonspherical fragments, perhaps tumbling flat plates. Alternative atmospheric models could be included to determine model robustness (Reference 32). The strewn field module is amenable to both Type 1 and Type 2 improvements. Algorithmic refinements can be added to improve calculation of field area and hence mean fragment density. Improvements to the fragment ejection database would allow the strewn field to be modelled using nonuniform fragment densities, yielding better hazard assessment.

EXPANDED SCOPE

88.   The scope of the original study was to model fragmentation, re-entry and strewn field formation mathematically in a 'first-order' approximation, sufficient to describe the principal processes at work. Opportunities for expanding the scope of the constituent modules have been discussed above. There are several possibilities for expanding the scope of the entire simulation. For example, the interpretation of the debris field as a hazard is unclear. This is especially so when considering the fields resulting from multiple intercepts of several Re-entry Vehicles. The debris fields can be interpreted as averaged, cumulative or otherwise weighted. Any of these interpretations are problematic. A uniform methodology for standard debris hazard assessment would be useful.

IMPROVED INTEROPERABILITY

89.   The strewn debris model was designed to accept input data provided by the ballistic missile intercept program (BMDKILL) developed within DAOR. As such, interoperability with BMDKILL is not an issue. However, the model could be enhanced to allow easy interfacing with other simulation packages modelling Theatre (as opposed to Intercontinental) Ballistic Missile Defence. Both in-house simulation packages such as TMDPAK (Reference 1) and comprehensive models such as EADSIM (Reference 33) could benefit from a complementary debris hazard assessment. Interest in debris following collisional or explosive destruction of Theatre Ballistic Missiles was sparked during the Gulf War (References 34,35) and is currently a topic of intense interest (References 4,6,9).

VI. CONCLUSION

90.   This Research Note documents a computer-based model for predicting the likely extent of the strewn debris field resulting from the interception of a ballistic missile Re-entry Vehicle by a hypervelocity kinetic kill Interception Vehicle.   The study considers the effect of exoatmospheric interception of Intercontinental Ballistic Missiles (at altitudes of hundreds of kilometres), although the effects of Theatre Ballistic Missile interceptions can be as easily considered. The intent of the study is to simulate Re-entry Vehicle destruction and to model the consequences of Ballistic Missile Defence. By using a 'first order' simulation, enough detail is included for the model to serve either as an aid to policy or strategic studies, or as a precursor to a more detailed engineering or systems analysis.

91.   The simulation package consists of mathematical descriptions of three processes: Re-entry Vehicle fragmentation through impact with the Interception Vehicle; fragment re-entry into the Earth's atmosphere; and eventual deposition of the fragments on the Earth's surface to form a strewn debris field.   Each stage is modelled at a mutually consistent level of detail.   The fragmentation module accepts as input position and velocity vectors of the Re-entry and Interception Vehicles, and simulates collisional fragmentation using a mass/velocity distribution based on laboratory and on-orbit observation of satellite/debris collisions. This module provides fragment initial conditions to the re-entry module, which generates ballistic fragment trajectories by numerical integration of the equations of motion governing motion in an ablative, exponentially dense atmosphere.   Fragment trajectories are followed to impact on the Earth's surface, where they are passed over to the final module, the strewn field module. This collates all fragment impact points and forms their convex hull, the minimal convex polygon containing all impact points, as an approximation to the actual strewn debris field. The modules have been implemented to run on both PC (DOS) and SUN (UNIX) platforms as *SDF_SIM*. An extended package, *CSDF_SIM*, models composite debris fields resulting from multiple engagements. A graphics package *(SDF_VIEW)* displays single and multiple strewn fields.

92.   This study did not address specific scenarios; however several general comments can be made concerning the probable extent of the debris field.   Ballistic missile interception is accompanied by tremendous amounts of kinetic energy. A 1000 kg Re-entry Vehicle travelling 5 km/sec colliding head-on with a 10 kg Interceptor travelling at the same speed results in 100 megajoules kinetic energy in the RV rest frame: this is approximately equal to the kinetic energy of ten fully-loaded C-130's at takeoff speed.   Laboratory experiments have shown that a significant fraction (on the order of one half) of this energy goes into producing and ejecting fragments. Hypervelocity collision results in the production of a very large number of very small (less than 1 gm) fragments travelling at several kilometres per second, and a small number of larger fragments (on the order of 1 kg) travelling at a few metres per second.   As ICBM intercepts typically occur a few hundred seconds before RV impact, this infers a large strewn debris field, on the order of a few hundred to a thousand kilometres radius. This also infers a low expected fragment density, on the order of grams per square kilometre. This heuristic approach is borne out by the model, which also takes atmospheric deceleration and mass ablation into account. The size, shape, and density of the strewn field is sensitively dependent upon the intercept conditions.

93.   In summary, the simulation currently serves as a basic assessment tool, providing estimates of the strewn debris field resulting from ballistic missile interception. The constituent processes are modelled at a level of detail sufficient to augment strategy or policy studies, or to act as a precursor to more detailed systems or engineering-level investigations.

VII. REFERENCES

1. Frank, G.W., *TMDPAK: A Theatre Ballistic Missile Defence Simulation Package,* Operational Research and Analysis Directorate of Air Operational Research Note 94/1, January 1994.

2. Dixson, M., G.W. Frank, *BMDKILL: A Ballistic Missile Interception Algorithm,* Directorate of Air Operational Project Report (in preparation).

3. Frank, G.W., Dixson,M, *Technical Modelling of North American Extended Air Defence Options,* Operational Research and Analysis Project Report 664, November 1994.

4. Cooper, H.F. (Ambass.), *Strategic Defence Initiative Global Protection Against Limited Strikes,* Strategic Defence Initiative Organization (Briefing, March 1992).

5. Israel, D.R., *Theatre Missile Defence Initiative TMD Programme Overview,* Ballistic Missile Defence Organization (Briefing, Assistance Deputy for Theatre Missile Defence BMDO, December 1993).

6. Ely, N.M. (LCol), National Missile Defence Program Briefing, Ballistic Missile Defence Organization (Briefing, National Missile Defence Directorate BMDO, December 1993).

7. Lennox, D., *ATBMs and Beyond,* Jane's Defence Weekly (22 May 1993) 21.

8. *ERINT Hits RV in Key ATBM Test,* Aviation Week and Space Technology (6 December 1993) 62.

9. Hughes, D., *ERINT Hits Storm RV Posing as Chemical Threat,* Aviation Week and Space Technology (December 13 1993) 57.

10. *Jane's Strategic Weapon Systems,* Ed. D. Lennox, Jane's Information Group (Alexandria Virginia 1993).

11. Scott, W.B., *LEAP Begins Flight Tests to Demonstrate Kinetic Kill Missile Defence Capability,* Aviation Week and Space Technology (17 June 1991) 207.

12. McKnight, D.S., *Determination of Breakup Initial Conditions,* J. Spacecraft 28 4 (July-August 1991) 470-477.

13. McKnight, D.S., Brechin, C.B., *Debris Creation via Hypervelocity Impact*, AIAA Paper 90-0084, January 1990.

14. Voyzelle, B., S. Belanger, C. Bourget, *Evaluation of the Sampling and Recovery Techniques Developed for the Radar Fragmentation Characterization Method*, Defence Research Establishment Valcartier (DREV R-4442/87) September 1987.

15. Allen, H. Julian, A.J. Eggers, Jr., *A Study of the Motion and Aerodynamic Heating of Ballistic Missiles Entering the Earth's Atmosphere at High Supersonic Speeds*, National Advisory Committee for Aeronautics Technical Report 1381 (1958).

16. Bate, Roger R., Donald D. Mueller, Jerry E. White, *Fundamentals of Astrodynamics*, Dover Publications (New York New York 1971).

17. *Basic Constants*, United States Air Force Aerospace Defence Command Space Computational Center, Program Documentation 1 January 1977.

18. Rabenstein, A.L., *Introduction to Ordinary Differential Equations* (Second Edition), Academic Press (New York New York 1972).

19. Vinh, Nguyen X., Adolf Busemann, Robert D. Culp, *Hypersonic and Planetary Entry Flight Mechanics*, University of Michigan Press (Ann Arbor 1980).

20. Chapman, Dean R., *An Approximate Analytical Method for Studying Entry into Planetary Atmospheres*, National Advisory Committee for Aeronautics Technical Report 4276 (1961).

21. Passey, Quinn R., H.J. Melosh, *Effects of Atmospheric Breakup on Crater Field Formation*, Icarus 42, 211-253 (1980).

22. *CRC Handbook of Chemistry and Physics*, 73rd Edition, David R. Lide Editor-in-Chief, CRC Press (London 1993).

23. Press, W.H., B.P. Flannery, S.A. Teukolsky, W.T. Vetterling, *Numerical Recipes, the Art of Scientific Computing* (Cambridge University Press, New York 1986).

24. Frank, G.W., M.A.H. Nerenberg, *Reconstructing the Attractor: A Review of Chaotic Time Series Analysis*, Canadian Journal of Physics, February 1991.

25. Sedgewick, R., *Algorithms* (Addison-Wesley London 1983).

26. Syck, J., *Turbo Pascal How-To*, The Waite Group (San Francisco 1992).

27. Frank, G.W., *Mathematics and Modelling of Orbital Motion*, Directorate of Air Operational Research Project Report (in preparation).

28. Goldstein, H., *Classical Mechanics*, Second Edition (Addison Weseley New York 1980).

29. *Turbo Pascal Version 6.0 Programmer's Guide*, Borland International (Scotts Valley California 1990).

30. Law, M.A., W.D. Keller, *Simulation Modelling and Analysis*, McGraw-Hill (New York New York 1991).

31. Harkey, W.B., *Re-Entry Aerodynamics*, AIAA Education Series 36 (AIAA 1988).

32. Bauer, E., *Standard Atmospheres for Engagement Modelling (U)*, Institude for Defense Analyses (Alexandria Virginia 1993).

33. *Extended Air Defence Simulation (EADSIM) Executive Summary*, U.S. Army Space and Strategic Defence Command Testbed Product Office, Huntsville Alabama (February 1993).

34. Postol, T.A., *Lessons of the Gulf War Experience with Patriot*, International Security, Winter 1991/92 (Vol. 16, No. 3) 119.

35. Stein, R.M., *Patriot ATBM Experience in the Gulf War (Draft)*, Missile Systems Division Advanced Air Defence Programs, Raytheon Company (Bedford MA 1992).

DOCUMENT CONTROL DATA	
(Security classification of title, body of abstract and indexing annotation must be entered when the overall document is classified)	

1. ORIGINATOR (the name and address of the organization preparing the document. Organizations for whom the document was prepared e.g. Establishment Sponsoring a contractor's report, or tasking agency, are entered in Section 8). OPERATIONAL RESEARCH & ANALYSIS DIRECTORATE OF AIR OPERATIONAL RESEARCH	2. SECURITY CLASSIFICATION (overall security classification of the document, including special warning terms if applicable) UNCLASSIFIED

3. TITLE (the complete document title as indicated on the title page. Its classification should be indicated by the appropriate abbreviation (S, C or U) in parentheses after the title)

FIRST-ORDER SIMULATION OF STREWN DEBRIS FIELDS ACCOMPANYING EXOATMOSPHERIC RE-ENTRY VEHICLE FRAGMENTATION BY HYPERVELOCITY IMPACT

4. AUTHORS (last name, first name, middle initial)

FRANK, GREGORY W.

5. DATE OF PUBLICATION (month Year of Publication of document) SEPT 1994	6a. NO. OF PAGES (total containing information. Include Annexes, Appendices, etc.) 72	6b. NO. OF REFS (total cited in document) 35

7. DESCRIPTIVE NOTES (the category of document, e.g. technical report, technical note or memorandum. If appropriate, enter the type of report e.g. interim, progress, summary, annual or final. Give the inclusive dates when a specific reporting period is covered.)

DAOR RESEARCH NOTE 94/5

8. SPONSORING ACTIVITY (the name of the department project office or laboratory sponsoring the research and development. Include the address).

ADM (Pol & Comm)

9a. PROJECT OR GRANT NO. (if appropriate, the applicable research and development project or grant number under which the document was written. Please specify whether project or grant.) DAOR PROJECT 23213 - ANALYSIS OF SPACE-RELATED AND SPACE SYSTEMS	9b. CONTRACT NO. (if appropriate, the applicable number under which the document was written.)
10a. ORIGINATOR's document number (the official document number by which the document is identified by the originating activity. This number must be unique to this document.) DAOR RESEARCH NOTE 94/5	10b. OTHER DOCUMENT NOS. (Any other numbers which may be assigned this document either by the originator or by the sponsor.)

11. DOCUMENT AVAILABILITY (any limitations on further dissemination of the document, other than those imposed by security classification.)

    (X) Unlimited distribution
    ( ) Distribution limited to defence departments and defence contractors: further distribution only as approved
    ( ) Distribution limited to defence departments and Canadian defence contractors; further distribution only as approved
    ( ) Distribution limited to government departments and agencies; further distribution only as approved
    ( ) Distribution limited to defence departments; further distribution only as approved
    ( ) Other (please specify):

12. DOCUMENT ANNOUNCEMENT (any limitation to the bibliographic announcement of this document. This will normally correspond to the Document Availability (11). However, where further distribution (beyond the audience specified in 11) is possible, a wider announcement audience may be selected.)

13. ABSTRACT (a brief and factual summary of the document. It may also appear elsewhere in the body of the document itself. It is highly desirable that the abstract of classified documents be unclassified. Each paragraph of the abstract shall begin with an indication of the security classification of the information in the paragraph (unless the document itself is unclassified) represented as (S), (C), or (U). It is not necessary to include here abstracts in both official languages unless the text is bilingual).

This report documents a computer-based model to simulate the strewn debris field resulting from exoatmospheric ballistic missile interception by a hypervelocity kinetic kill vehicle. The model supports a suite of simulations developed to augment policy or strategic studies by capturing the basic physics of missile defence. The model is intended to serve as a "first order" approximation, describing physical processes at a level of detail sufficient to describe strewn field formation qualitatively. This report is a technical document of the physics underlying fragmentation and dispersion, and is intended for analysts working with or expanding the package. Fragmentation of ballistic missile re-entry vehicles is modelled using available information from satellite on-orbit and laboratory collisions. Atmospheric fragment re-entry is modelled using an exponentially dense ablative atmospheric model derived from meteor physics. Strewn field distributions are inferred through impact points across a range of fragment masses. Follow-on analysis packages compute and display mean and cumulative fragment densities accompanying multiple intercept scenarios. While this study did not address specific scenarios, several trends have emerged: interceptions may occur at altitudes of hundred of kilometres, several hundred seconds before scheduled RV impact. Such interceptions are often characterized by debris fields measuring several hundreds of kilometres across. Assuming uniform fragment distribution yields low mean fragment mass densities on the order of a few grams per square kilometre.

14. KEYWORDS, DESCRIPTORS or IDENTIFIERS (technically meaningful terms or short phrases that characterize a document and could be helpful in cataloguing the document. They should be selected so that no security classification is required. Identifiers, such as equipment model designation, trade name, military project code name, geographic location may also be included. If possible keywords should be selected from a published thesaurus, e.g. Thesaurus of Engineering and Scientific Terms (TEST) and that thesaurus-identified. If it is not possible to select indexing terms which are Unclassified, the classification of each should be indicated as with the title.)

Anti Missile Defence Systems
Atmospheric Re-Entry
Ballistic Missile Intercept Systems
Collisional Fragmentation
Computer Model
Computer Simulation
Fragmentation
Hypervelocity Impact
Hypervelocity Weapons
Kinetic Energy Weapons
Mathematical Model
Strategic Missile Defence
Strewn Debris Field
Theatre Missile Defence

Canada